Experiments on animals and animal tissues

It is a requirement of The Society that all vertebrates (and Octopus vulgaris) used in experiments are humanely treated and, where relevant, humanely killed.

To this end authors must tick the appropriate box to confirm that:

For work conducted in the UK, all procedures accorded with current UK legislation.

For work conducted elsewhere, all procedures accorded with current national legislation/guidelines or, in their absence, with current local guidelines.

Experiments on humans or human tissue

Authors must tick the appropriate box to confirm that:

All procedures accorded with the ethical standards of the relevant national, institutional or other body responsible for human research and experimentation, and with the principles of the World Medical Association's Declaration of Helsinki.

Guidelines on the Submission and Presentation of Abstracts

Please note, to constitute an acceptable abstract, The Society requires the following ethical criteria to be met. To be acceptable for publication, experiments on living vertebrates and Octopus vulgaris must conform with the ethical requirements of The Society regarding relevant authorisation, as indicated in Step 2 of submission.

Abstracts of Communications or Demonstrations must state the type of animal used (common name or genus, including man. Where applicable, abstracts must specify the anaesthetics used, and their doses and route of administration, for all experimental procedures (including preparative surgery, e.g. ovariectomy, decerebration, etc.).

For experiments involving neuromuscular blockade, the abstract must give the type and dose, plus the methods used to monitor the adequacy of anaesthesia during blockade (or refer to a paper with these details). For the preparation of isolated tissues, including primary cultures and brain slices, the method of killing (e.g. terminal anaesthesia) is required only if scientifically relevant. In experiments where genes are expressed in Xenopus oocytes, full details of the oocyte collection are not necessary. All procedures on human subjects or human tissue must accord with the ethical requirements of The Society regarding relevant authorisation, as indicated in Step 2 of submission; authors must tick the appropriate box to indicate compliance.

SA01

Manipulating the peripheral nervous system to affect microvascular perfusion and metabolic health

Erin Paley[1], MariKate Murphy[1], Kayla Mac[1], Caroline Geisler[2], Jonathan Davis[3], Benjamin Renquist[1]

[1]University of Arizona, United States of America, [2]University of Kentucky, United States of America, [3]The Ohio State University, United States of America

Diabetes and the associated hyper- and hypo-glycemia damage blood vessels in the brain, worsening cognitive function and increasing the risk of developing dementia. Type 2 diabetes mellitus is characterized by insulin resistance. The “resistance” to insulin is largely a result of poor insulin delivery to the target cells with blood flow being the primary regulator of insulin mediated glucose update. Blood flow to skeletal muscle is tightly regulated by both the vasoconstrictive, sympathetic and vasodilatory, parasympathetic nervous systems.

We are taking advantage of the interorgan communication facilitated by the peripheral nervous system to manipulate blood flow to improve glucose homeostasis.

The baroreceptor reflex is defined as the sensing of pressure in the aortic arch and compensatory changes in vascular tone and heart rate to maintain blood pressure. Using a mouse with improved cardiac contractility, we activated the baroreceptor reflex, to induce vasodilation and improve glucose homeostasis in diet-induced obese mice.

Fatty liver is associated with hypertension and insulin resistance. We previously established that the fatty liver produces GABA, which inhibits activity of the vagal nerve resulting in hyperinsulinemia and insulin resistance. Inhibiting liver GABA production improves insulin sensitivity, prevents obesity and angiotensin II induced hypertension, and increases vasodilatory cGMP in skeletal muscle. GABA signaling onto the hepatic vagal nerve increases peroneal nerve activity and sympathetic tone at skeletal muscle. This established the key role of hepatic vagal afferent signaling in regulating insulin and glucose delivery to skeletal muscle.

Together our studies establish the potential to target the afferent peripheral nervous system signaling to modulate microvascular blood flow, systemic blood pressure, and metabolic health.

SA02

Mind over MASLD: Unravelling brain dysfunction in steatotic liver disease

Anna Hadjihambi[1]

[1]Roger Williams Institute of Liver Studies, School of Immunology & Microbial Sciences, Faculty of Life Sciences and Medicine, King's College London, Foundation for Liver Research and King's College Hospital, London., United Kingdom

Metabolic dysfunction–associated steatotic liver disease (MASLD) is a chronic multisystem disease affecting approximately 30% of the general population and more than 80% of individuals with obesity. It frequently coexists with cardiovascular disease, diabetes, and cancer, contributing to a growing global burden of multimorbidity. While hepatic encephalopathy is classically associated with advanced liver disease, accumulating evidence indicates that neurocognitive impairment and accelerated brain ageing also occur in earlier stages of MASLD. However, the mechanisms driving these cerebral alterations, and whether they are reversible following disease resolution, remain largely unknown.

In this talk, data will be presented from male C57BL/6NTac mice fed a control diet (CD) or a high-fat, high-cholesterol diet (HFD) for 26 weeks to induce MASLD. To assess the impact of ageing and dietary intervention, a subset of HFD-fed mice was subsequently switched to a low-fat diet (LFD) and followed until 18 months of age. All animal procedures were carried out in accordance with the UK Animals (Scientific Procedures) Act 1986 and its associated guidelines, and complied with the ARRIVE guidelines. The study was conducted under a UK Home Office Project Licence and approved by the local Animal Welfare and Ethical Review Body (AWERB). All efforts were made to minimise animal suffering and to reduce the number of animals used.

Behavioural analyses revealed anxiety-like behaviour in both HFD and aged HFD-LFD mice, while memory impairment was evident in aged CD-LFD and HFD-LFD groups.Measurements of brain oxygenation showed reduced partial pressure of oxygen and tissue oxygen saturation in HFD, aged HFD-LFD, and CD-LFD mice at baseline, assessed under anaesthesia using fluorescence-based methods and optoacoustic tomography. Cerebrovascular reactivity to systemic hypercapnia (10% CO_2) was preserved. Structural analyses demonstrated altered vascular complexity and reduced pericyte coverage in HFD and aged HFD-LFD mice compared to controls. These changes were accompanied by increased cortical microglial density, coverage, and volume, consistent with a reactive inflammatory phenotype.

Together, these findings identify altered brain oxygenation and inflammation as potential contributors to MASLD-associated brain dysfunction. Importantly, dietary fat reduction in later life did not reverse MASLD or its associated cerebral alterations, suggesting that brain vulnerability may persist or even be exacerbated with ageing. Ongoing studies in mice of both sexes are currently exploring alternative dietary strategies and mechanisms acting along the gut-liver–brain axis. This work aims to define the long-term impact of MASLD on brain health, even after liver disease improvement, and to understand how metabolic liver disease interacts with the natural ageing process.

SA03

Using microfluidic models to explore vascular responses in CSVD and stroke

Paul Holloway[1]

[1]University of Oxford, United Kingdom

Introduction

Stroke and cerebral small vessel disease (CSVD) are major causes of death and disability worldwide. Cerebral Small Vessel Disease is a group of conditions that affects the stability of cerebral micro-vessels, manifesting in a variety of clinical syndromes, including vascular cognitive impairment, dementia, and stroke. CSVD accounts for a quarter of the 12 million global stroke cases, and ~45% of the 35–42 million new cases of dementia each year (Bos et al, 2018). Despite the world-wide importance of CSVD and stroke there are no current treatments beyond risk factor modification and restoration of blood flow. A major barrier to developing new therapies is a lack of relevant human in vitro models that capture the form and function of brain blood vessels. Our lab is developing new models of both stroke and CSVD that enable the study of cerebral blood vessel function and dysfunction.

Aims

To develop a suit of microfluidic cell culture models that replicate blood vessel dysfunction in CSVD and stroke.

Methods

We have used soft-lithography micro-fabrication techniques to produce microfluidic cell culture devices that can pattern a cell laden hydrogel and stimulate vasculogenesis to create a capillary network mimetic. To model stroke, human primary brain endothelial cells, pericytes and astrocytes were co-cultured and allowed to form vessel like structures before being subjected to oxygen glucose deprivation. Vessel integrity was measured using fluorescent tracer dyes. For CSVD models, induced pluripotent stem cells were derived from patients with monogenic forms of CSVD and differentiated to endothelial cells, pericytes and astrocytes for co-culture in microfluidic devices. Barrier integrity of the resulting in vitro vessels was measured using fluorescent tracers and compared to isogenic disease corrected controls.

Results

Both stroke mimicking conditions and CSVD causing mutations disrupted barrier function of in vitro brain capillary networks.

Conclusions

Microfluidic cell culture approaches can be used to create brain capillary mimetics that recapitulate barrier disruption relating to stroke and CSVD.

SA04

Inflammation before and after the bleed: A dual role for cholesterol in intracerebral haemorrhage?

Paul Kasher[1]

[1]The University of Manchester, UK

Intracerebral haemorrhage (ICH) is a severe form of stroke caused by spontaneous blood vessel rupture and bleeding into the brain tissue, resulting in significant disability and death. Our research, using in vitro systems, post-mortem brain tissue, zebrafish, and mouse models, has identified Cholesterol 25-hydroxylase (Ch25h) as a critical molecule influencing both the risk of ICH and the brain's response to injury after a bleed.

Systemic infections and inflammation can compromise neurovascular integrity, increasing the risk of blood vessel rupture and ICH in some people (1). While infection-induced hypertension and endothelial dysfunction are known contributors, hypocholesterolemia—low levels of LDL cholesterol—is a less understood but clinically relevant risk factor (2). Cells respond to infection by temporarily reducing cholesterol availability, which can impair the formation and function of adherens junctions and may destabilise the neuroendothelium (3, 4). We hypothesise that this infection-driven cholesterol dysregulation can, under certain conditions, lead to neurovascular instability and ICH.

After ICH occurs, the influx of blood into the brain triggers widespread inflammation and cellular damage. Reactive oxygen species, iron from haemoglobin breakdown, and cellular debris activate microglia and recruit peripheral leukocytes, amplifying injury. Cholesterol metabolism plays a dual role in this context: disrupted lipid handling can intensify inflammation, while efficient cholesterol clearance supports tissue repair. Cholesterol is also essential for membrane synthesis and remyelination, making its regulation a delicate balance between injury and recovery.

Ch25h is an enzyme that converts cholesterol into 25-hydroxycholesterol (25HC), an oxysterol involved in immune regulation. We found that antiviral signalling increases Ch25h expression in zebrafish and human foetal brain tissue, correlating with ICH risk. In brain endothelial cell cultures and zebrafish models, Ch25h and 25HC disrupt vascular integrity by remodelling cholesterol metabolism (5). This suggests a mechanistic link between infection, cholesterol dysregulation, and neurovascular dysfunction. As well as its role in ICH risk, Ch25h also influences recovery after brain haemorrhage. In both mouse and human brain, Ch25h is strongly upregulated in microglia and macrophages after ICH. Loss of Ch25h in mice worsens outcomes, while treatment with 25HC enhances blood clearance and improves acute recovery. We also show 25HC regulates lipid droplet accumulation in macrophages following phagocytosis of red blood cells, indicating a broader role in lipid handling during haematoma clearance.

In summary, Ch25h and its product 25HC are central to both the onset and resolution of ICH. They mediate neurovascular dysfunction during infection and regulate immune and lipid responses during brain injury and recovery. Targeting this pathway may offer new preventative and therapeutic strategies to reduce ICH risk and improve outcomes, respectively.

SA05

Redox regulation of neurovascular coupling in health and disease

Cátia Lourenço[1]

[1]University of Coimbra, Portugal

The functional integrity of the brain depends on a tight coupling between neuronal activity and local cerebral blood flow, a process known as neurovascular coupling (NVC). This mechanism ensures the timely delivery of oxygen and metabolic substrates to active neuronal circuits. Nitric oxide (NO), produced through the glutamate–NMDAr–nNOS–sGC pathway, is a key mediator of communication between neurons and the cerebral vasculature. Under physiological conditions, tightly controlled redox signaling preserves NO bioavailability and supports efficient NVC. Conversely, disruption of redox homeostasis reduces NO bioavailability which is linked to NVC impairment and cognitive decline in different pathological conditions (e.g. Alzheimer's disease, vascular cognitive impairment and type 2 diabetes). Understanding how redox mechanisms regulate NO signaling within the neurovascular unit is therefore critical for identifying strategies capable of preserving cerebrovascular function and cognitive health. Among these, dietary inorganic nitrate—abundant in vegetables such as beetroot and green leafy vegetables—has emerged as a promising approach to enhance NO bioavailability.

To explore the interplay between redox regulation, NO signaling, neurovascular coupling and cognition, we investigated rodent models of vascular cognitive impairment, including chronic cerebral hypoperfusion (2VO) and type 2 diabetes. Using a multimodal approach combining behavioral testing, in vivo assessment of NVC and cerebral blood flow dynamics, magnetic resonance imaging, and molecular analyses of vascular remodeling and oxidative stress pathways, we demonstrate that these models exhibit marked neurovascular dysfunction accompanied by oxidative stress–driven redox imbalance and impaired spatial learning and memory. Importantly, boosting NO bioavailability through dietary nitrate was able to improve NVC responses, improved cerebral blood flow regulation, attenuated pathological vascular remodeling, and improved cognitive performance. Together, these findings highlight the central role of redox-dependent regulation of NO signaling in maintaining neurovascular coupling in health and its disruption in disease.

SA06

Cerebrovascular Dynamics in Dementia: Exploring Dysfunctional Brain Cell Interactions

Axel Montagne[1]

[1]The University of Edinburgh, United Kingdom

Cerebral small vessel disease (SVD) is a leading contributor to dementia and stroke, with pathology centred on the brain's microvasculature. Increasing evidence highlights the role of endothelial activation, pericyte dysfunction, blood–brain barrier (BBB) dysfunction, and inflammatory responses in driving disease onset and progression. Importantly, many of these vascular mechanisms are also implicated in Alzheimer's disease (AD), pointing to overlapping pathways of neurovascular dysfunction across dementias.

In our lab, we combine translational approaches across human and preclinical models to investigate these mechanisms. Using advanced imaging, we assessed age-related and disease-associated changes in pericyte and endothelial function in both mouse and human brain tissue. Circulating vascular biomarkers were evaluated in patient cohorts and correlated with MRI features of SVD. Complementary experimental models in mice, including endothelial- and pericyte-targeted manipulations, were used to probe causal relationships between vascular dysfunction, BBB integrity, and microglial responses.

Together, these investigations reveal the importance of endothelial–pericyte crosstalk in vascular vulnerability and highlight conserved mechanisms across species. This integrated strategy advances our understanding of SVD pathophysiology and its overlap with AD, identifying potential avenues for biomarker development and therapeutic intervention across neurodegenerative diseases.

SA07

BACE1: A novel regulator of the microcirculation from head to toe

Paul Meakin[1], Max Lester[1], Siobhan Beastall[1], Lia Pinto[1], Amanda MacCannell[1]

[1]University of Leeds, United Kingdom

Metabolic disease (Type 2 diabetes and obesity), neurodegeneration and auto-immune diseases are all characterised by chronic inflammation. We are interested in the vascular consequences of inflammation by understanding the molecular mechanisms involved. Vascular inflammation is a complex immune response occurring in blood vessels, characterised by endothelial dysfunction, activation of immune cells and perivascular adipose tissue and the release of proinflammatory chemokines and cytokines. Damaged blood vessels increased risk of developing cardiovascular diseases which is a precursor to vascular complications including atherosclerosis, heat attack and stroke.

The protease β-site APP-cleaving enzyme 1 (BACE1) is associated with Alzheimer's disease development, via the production of β-amyloid peptides. However, our work using proteomics and RNAseq analysis has shown increased BACE1 activity drives endothelial dysfunction. Furthermore, we have identified genetic associations with hyperlipidaemia and hypertension. Here we explore the hypothesis that BACE1 could be a novel drug target for vascular disease.

Results: BACE1 is highly expressed in endothelial and smooth muscle cells in human atherosclerotic lesions. With elevated expression occurring in the early phases of lesion development.

Four-week treatment of a BACE1 inhibitor (Merck-3) in Western diet fed ApoE KO mice reduced atherosclerotic plaque load by 50% both in the whole aorta and aortic root ($P<0.05$). Furthermore, BACE1 inhibition lowered vascular inflammation ($P< 0.01$), serum triglyceride ($P< 0.01$) and LDL cholesterol ($P< 0.05$) levels and reduced hypertension ($P< 0.05$) compared to vehicle controls. Mechanistically, BACE1 inhibition restores endothelial cells and vascular function.

Conclusions: Taken together our data demonstrate that elevated BACE1 activity is a driving factor of atherosclerotic lesion development via induction of endothelial dysfunction. Thus, targeting this with available BACE1 inhibitors could be a novel therapy for atherosclerosis and vascular disease. These findings have the potential to have wide ranging impact as the interrelation of blood vessels, inflammation and immunity is a fundamental physiological process while also underlying several diseases, ranging from infections to autoimmune diseases, metabolic syndrome, dementia.

SA08

Blood flow changes and myelin damage as early mechanisms leading the dementia

David Attwell[1]

[1]University College London, United Kingdom

Both Alzheimer's disease and vascular dementia are associated with a decrease in cerebral blood flow, which will disrupt neuronal function. I will give an overview of how these blood flow decreases occur, and then describe early effects of low blood flow and of amyloid beta production on myelinated axons. I will show that the node of Ranvier gets longer with low cerebral blood flow and with amyloid beta release, and that this is associated with myelin damage. The mechanisms of these effects will be assessed, with the aim of identifying a possible therapeutic approach for preventing disruption of the function of myelinated axons.

C01

Cross-sectional Associations Between Sleep Quality and Glucose Regulation in Older Adults

Sophie Berghmans[1], Connor Snow[1], Matiram Pun[1], Elnaz Ehteshami Afshar[1], Jean M. Rawling[1], Jessalyn K. Holodinsky[1], Jamie Benham[1], Willis H. Tsai[1], Michael D. Hill[1], Ronald Sigal[1], Marc J. Poulin[1]

[1]University of Calgary, Canada

Introduction

Sleep quality, glucose regulation, and age-related metabolic changes converge on physiological pathways linked to cognitive decline across the lifespan. More than 500 million adults worldwide meet criteria for impaired glucose regulation, highlighting the scale of metabolic vulnerability in aging populations[1]. Aging is also associated with altered sleep architecture, increased fragmentation, and higher apnea burden, all of which may contribute to metabolic and neurovascular risk[2]. Yet how sleep architecture (macro and microarchitecture) and sleep-disordered breathing relate to glucose regulation in aging, and whether these relationships differ by sex, remains incompletely understood.

Aims/Objectives

We investigated the relationship between traditional sleep architecture, sleep depth (Odds Ratio Product; ORP), and glucose regulation in community-dwelling middle-aged to older adults. We further examined whether these associations differed by sex.

Methods

The study conformed to the standards set by the Declaration of Helsinki. Eighty-six adults (n=56 women; age 63.8±5.9 years) from the Brain in Motion II study completed overnight in-home Level II polysomnography and fasting blood sampling. Glucose status was classified as normoglycemic (n=45; ≤5.6 mmol/L) or glucose-dysregulated (n=40; >5.6 mmol/L). Groups were comparable for age and sex.

Results

Individuals with glucose dysregulation had higher body mass index (30.8±4.9 *vs*. 27.3±5.1 kg/m^2; p=0.002), higher body fat percentage (38.1±7.1 *vs*. 35.1±7.2%; p<0.001), and lower $\dot{V}O_2$max (24.9±5.3 *vs*. 27.9±4.7 mL/kg/min; p=0.007). Glucose-dysregulated participants displayed higher sleep efficiency (76.5±10.1 *vs*. 70.2±10.4%; p=0.002), shorter sleep-onset latency (25.3±36.2 *vs*. 42.6±45.6 min; p=0.037), and less full wakefulness (ORP decile 10: 8.9±6.4 *vs*. 13.7±7.1% of total sleep time; p=0.002). Total sleep time (346.0±65.0 *vs*. 327.6±72.8 min; p=0.278) and wake after sleep onset (137.1±58.3 *vs*. 125.4±51.7 min; p=0.241), did not differ significantly between groups. No group differences were observed in other ORP deciles or NREM stages.

Sex-based analyses showed that females had higher sleep efficiency (75.0±10.4 *vs*. 69.8±10.9%; p=0.012), less time awake (115.4±52.4 *vs*. 141.0±60.5 min; p=0.018), and greater NREM stage 3 sleep (55.1±40.1 *vs*. 17.7±26.6 min; p<0.001) compared with males. Sex-by-glucose interactions indicated that differences in sleep efficiency and wakefulness by glucose status were evident in females but not males.

Overall, apnea–hypopnea index (AHI) did not differ by glucose group or sex; however, glucose-dysregulated females exhibited higher AHI than normoglycemic females (26.1±16.8 *vs*. 15.7±11.9 events·h^{-1}, p=0.046). When categorized by OSA severity, glucose-dysregulated participants showed a

greater burden of moderate-to-severe OSA, whereas normoglycemic participants were more likely to fall within no or mild OSA categories. Hypoxia-related indices were also worse in glucose-dysregulated participants, particularly among females.

Conclusion

Our findings suggest that the relationship between glucose regulation and sleep in older adults is more nuanced than expected. Glucose-dysregulated participants exhibited patterns consistent with increased homeostatic sleep pressure, including higher sleep efficiency and reduced wakefulness, potentially reflecting early physiological adaptations preceding overt sleep disruption. The paradoxically "better" sleep outcomes may be influenced by higher BMI and a greater burden of undiagnosed mild-to-moderate OSA, with chronic sleep fragmentation, REM disruption, and nocturnal hypoxia contributing to compensatory sleep drive. This underscores the importance of considering sleep-disordered breathing when evaluating sleep–glucose interactions and may inform early preventive strategies targeting both metabolic and sleep pathways to support healthy aging.

C02

Acute Intestinal Inflammation Alters Cerebral Hemodynamic Stability and Functional Connectivity in Mice

Zheqin Li[1], Kieron South[1], Craig Smith[1], Stuart Allan[1]

[1]University of Manchester, United Kingdom

Introduction

Inflammatory bowel disease (IBD), primarily Crohn's disease and ulcerative colitis, is an immune-mediated inflammatory disorder of the gastrointestinal tract. Beyond intestinal pathology, individuals with IBD frequently experience extra-intestinal manifestations and have an increased risk of cerebrovascular events, potentially driven by systemic inflammation and prothrombotic mechanisms. Using a dextran sulphate sodium (DSS)-induced colitis model, we investigated whether acute intestinal inflammation is associated with systemic inflammatory changes and alterations in cerebral haemodynamics and functional connectivity assessed using functional ultrasound (fUS).

Methods

CD1 mice aged 4–8 weeks were allocated to acute DSS-induced colitis (5% w/v, 40 kDa DSS in drinking water for 3 days; n=20, 10 female) or control conditions (standard drinking water; n=20, 10 female). Disease activity index (DAI) was assessed daily using body weight change, stool consistency, and faecal occult blood testing. Following the 3-day exposure, mice underwent 15 minutes of resting-state fUS imaging (Iconeus One) under isoflurane anaesthesia. Blood was collected for plasma, and mice were perfusion-fixed with paraformaldehyde.

Faecal calprotectin and serum inflammatory/coagulation-related markers (IL-6, von Willebrand factor antigen [VWF:Ag], functional VWF activity [VWF:CBA], and ADAMTS13) were quantified using ELISA.

fUS was used to map cerebral blood volume (CBV) and functional connectivity across the brain. Twenty regions of interest (ROIs) were manually defined with reference to the Allen Mouse Brain Atlas. Baseline CBV was defined as the mean of the first 40 seconds; relative change (ΔCBV) was computed as (CBV − baseline)/baseline. ROI-wise ΔCBV time courses were extracted. Functional connectivity assessment was estimated from low-frequency (<0.1 Hz) fluctuations following detrending and confound removal. Group comparisons used t-tests, with family-wise error rate control via permutation testing (10,000 permutations); $p<0.05$ was considered significant. All procedures complied with the UK Animals (Scientific Procedures) Act 1986 and were approved by the University of Manchester ethical review board.

Results

DSS exposure induced clear intestinal and systemic inflammatory changes. DAI scores increased from day 1 and remained elevated through day 3 in the DSS group relative to controls (Figure 1a). Faecal calprotectin levels were significantly higher in DSS-treated mice, alongside increased serum IL-6 (Figure 1b-c). In contrast, coagulation-related markers (VWF:Ag, VWF:CBA, and ADAMTS13) did not differ significantly between groups (Figure 1d-h).

Resting-state fUS revealed a consistent but modest increase in mean ΔCBV in DSS-treated mice; however, no ROI survived permutation-based FWER correction. Notably, temporal association, auditory,

and ectorhinal cortices showed significantly greater temporal variability of ΔCBV (higher standard deviation over time), suggesting increased haemodynamic fluctuation (Figure 2). ROI-to-ROI connectivity analyses further identified significantly increased functional connectivity between auditory and ectorhinal regions in the DSS group. (Figure 3)

Conclusion

Acute DSS-induced colitis produced robust intestinal inflammation accompanied by systemic cytokine elevation and measurable alterations in resting-state cerebral haemodynamic dynamics. Although mean ΔCBV differences did not survive stringent multiple-comparison correction, increased temporal variability and enhanced connectivity between auditory and ectorhinal regions suggest that peripheral inflammation may modulate neurovascular dynamics. Further mechanistic work is warranted to clarify inflammation–brain coupling in IBD and its potential relevance to cerebrovascular vulnerability.

Figure 1

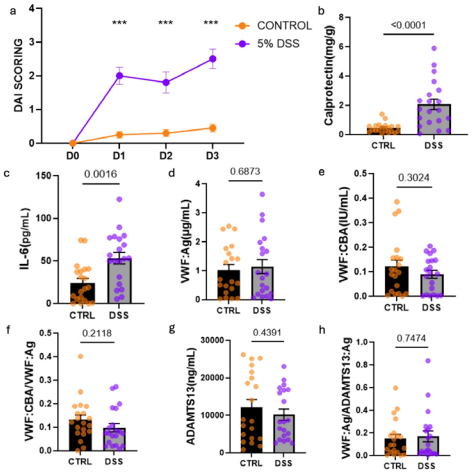

DSS treatment induces inflammation without altering coagulation markers. *(a) Disease Activity Index (DAI) scores were significantly elevated in the 5% DSS group compared to controls from day 1 through day 3. (b–c) Markers of inflammation were significantly upregulated in DSS-treated mice, shown by increased fecal calprotectin (b) and serum IL-6 levels (c). (d–h) Conversely, coagulation-related parameters—including VWF:Ag, VWF:CBA, ADAMTS13, and their associated ratios—showed no significant differences between the control and DSS groups.*

Figure 2

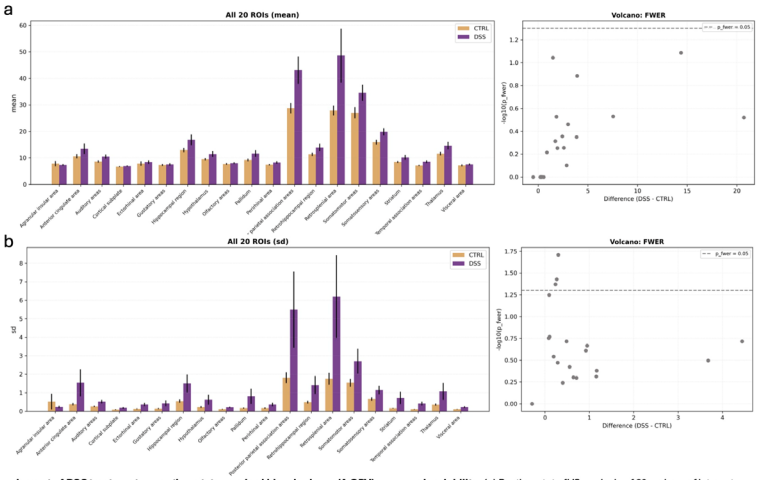

Impact of DSS treatment on resting-state cerebral blood volume (Δ CBV) mean and variability. *(a) Resting-state fUS analysis of 20 regions of interest (ROIs) indicated a consistent but modest trend toward increased mean Δ CBV in DSS-treated mice compared to controls. However, the volcano plot (right) confirms that no ROI survived permutation-based family-wise error rate (FWER) correction. (b) In contrast, analysis of signal fluctuation (standard deviation) revealed significantly higher temporal variability of Δ CBV in the DSS group. The temporal association, auditory, and ectorhinal cortices exhibited significantly increased variability that survived FWER correction (p.adjust < 0.05, points above the dashed line).*

Figure 3

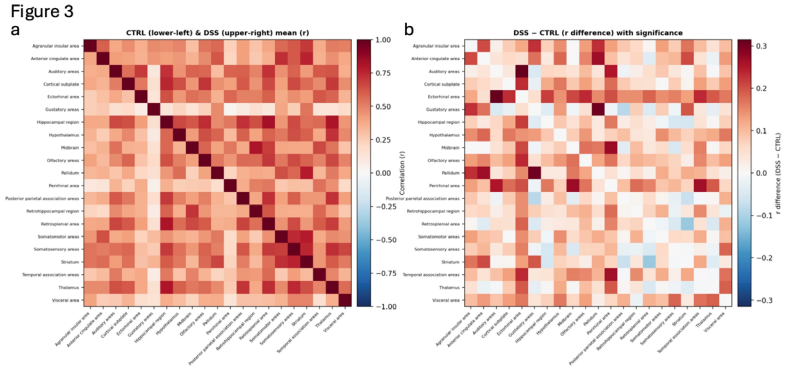

Alterations in ROI-to-ROI functional connectivity between control and DSS-treated mice. (a) Mean correlation matrix showing functional connectivity across 20 regions of interest (ROIs). The lower-left triangle represents the control group, while the upper-right triangle represents the DSS group. (b) Heatmap displaying the differential connectivity (DSS – Ctrl) where red indicates increased connectivity and blue indicates decreased connectivity in the DSS group. Statistical analysis revealed a significant increase in functional connectivity between the auditory and ectorhinal cortices in DSS-treated mice compared to controls.

C03

Does systemic microvascular function mediate the association between large artery stiffness and cognitive function in older adults?

Kunihiko Aizawa[1], Kim M Gooding[1], Francesco Casanova[1], David J Llewellyn[2], Andrew Forbes Brown[1], Natalia Rolinska[1], Anna Barnes[1], David M Mawson[1], Phillip E Gates[1], Mark Gilchrist[1], W David Strain[3], Angela C Shore[1]

[1]University of Exeter Medical School, NIHR Exeter Clinical Research Facility, UK, [2]University of Exeter Medical School, Alan Turing Institute , UK, [3]University of Exeter Medical School, NIHR Exeter Clinical Research Facility, Royal Devon University Healthcare NHS Foundation Trust, UK

INTRODUCTION: Previous research identified a link between increased large artery stiffness and adverse brain health, supporting the concept that the penetration of excess pulsatility into cerebral circulation damages its small vessels and, when persisted, leads to cognitive decline. Although assessing cerebral microvasculature non-invasively at bedside poses a major challenge, systemic microvascular function such as that of skin can be utilised to investigate the link. We determined whether large artery stiffness and systemic microvascular function were associated with cognitive function in older adults, and also determined whether systemic microvascular function mediated an association between large artery stiffness and cognitive function. **METHODS:** Older adults with diverse cardiovascular risk (n=435, 162 females) participated in this study. Estimated pulse wave velocity (ePWV) as an indirect estimate of large artery stiffness was calculated from age and mean arterial pressure as described elsewhere.[1] Systemic microvascular function was assessed by responses to pharmacological stimulation of forearm skin blood vessels using a solid-state laser Doppler imager (LDI2, Moor Instruments, Axminster, UK) as previously described.[2] Endothelium-dependent (acetylcholine: ACh) and -independent (sodium nitroprusside: SNP) vasodilators were delivered trans-dermally via iontophoresis, and forearm skin perfusion was measured as the area under the response curve of each vasodilator (ACh_auc and SNP_auc, respectively) normalised to resting perfusion. Validated cognitive tasks [Addenbrooke's Cognitive Examination Revised (ACE-R), Trail Making Test Part-A (TMT-A) and Part-B (TMT-B)] were administered to assess participants' global cognitive function, speed of processing and executive function, respectively. A higher total score for ACE-R and a shorter completion time for TMT-A and TMT-B indicate better functions. All procedures accorded with current UK legislation. **RESULTS:** One standard deviation (SD) increase in ePWV was positively associated with TMT-A [β=0.339 (0.226, 0.467), p<0.001] and TMT-B [β=0.342 (0.232, 0.451), p<0.001] after accounting for conventional cardiovascular risk factors. Additionally, one SD increase in ACh_auc was inversely associated with TMT-B after adjusting for conventional cardiovascular risk factors [β=-0.113 (-0.201, -0.024), p=0.013]. A mediation analysis revealed that the association between ePWV and TMT-B was partially mediated by ACh_auc explaining about 3% of the total effect in the unadjusted model (p<0.05), but this did not persist in the adjusted model. **CONCLUSIONS:** Large artery stiffness and systemic microvascular function were associated with cognitive function in older adults, but these vascular measures may independently contribute to cognitive function without systemic microvascular function mediating the association between large artery stiffness and cognitive function in our cohort.

C04

Effects of ageing, obesogenic diet, and the flavonoid Fisetin on small artery function in mice

Zhang Beijia[1], Line Fleischer Hach[2], Raquel Feliciano[2], Juliette Helene Gisele Laurence Tavenier[2], Wang Yu[3], Andersen Ove[2], Line Jee Hartmann Rasmussen[2], Lars Jørn Jensen[1]

[1]Department of Veterinary and Animal Sciences, University of Copenhagen, Denmark, [2]Department of Clinical Research, Copenhagen University Hospital Amager and Hvidovre, Denmark, [3]Department of Pharmacology and Pharmacy, The University of Hong Kong, Hong Kong SAR, China

In humans, ageing and metabolic stress involving a sedentary lifestyle and excess caloric intake are significant risk factors for developing cardiovascular, cerebrovascular, and neurodegenerative diseases. The pathophysiology of these diseases involves hypertension and/or dysregulation of blood flow in critical organs. Small (resistance) arteries (<300 µm) regulate tissue blood flow and systemic vascular resistance. Endothelial dysfunction, hypercontractility, deficient autoregulation, structural remodeling, and arterial stiffening are hallmarks of vascular dysfunction. The flavonoid fisetin has known cardioprotective activities, but it is unknown whether it can alleviate vascular dysfunction in ageing and metabolic stress. The primary objectives of this study were to investigate small artery dysfunction in young vs. old mice with or without diet-induced metabolic stress, and to test whether Fisetin can reverse vascular dysfunction. A secondary objective was to test if Rho-kinase is involved in age- or diet-induced vascular dysfunction.

Animal treatments and procedures were approved by the relevant authorities. Wildtype C57BL/6NTac male mice were divided into 8 groups evenly distributed to intermittent Fisetin or Vehicle treatment (4 weeks; 20 mg/kg 2 days/week). Young mice (3.5 months at study end) were fed either normal diet (N=16) or a high-fat diet (60% saturated fat) with fructose (10%) in drinking water (N=16) for 10 weeks. Old mice (retired breeders; 17 months at study end) were fed either normal chow (N=15) or a high-fat/high-fructose diet (N=15) for 10 weeks. At study end, mice were humanely sacrificed, and 3rd order mesenteric arteries (150-200 µm) were quickly dissected free from fat and connective tissue. Using a pressure myograph system, arteries were cannulated under physiological pressure (60 mm Hg) and bathed in Krebs buffer (37°C; pH 7.40). We measured the following vascular responses: vasoconstriction to high-KCl (75 mM K^+) and noradrenaline (NA, 1 µM); dilation to the endothelium-dependent vasodilator acetylcholine (ACh, 10 µM); myogenic tone (MT; pressure range 60-120 mm Hg); structural remodeling (passive lumen diameter, wall cross-sectional area, wall/lumen-ratio); and vascular stiffness (Young's Modulus). We also tested the effects of Rho-kinase inhibition (Ripasudil, 400 nM) on MT. We performed factor analysis with age and diet as factors (plus age x diet interaction) in vehicle- vs. Fisetin-treated mice, using two- or three-way Anova with multiple comparisons. A P-value <0.05 was considered significant.

Ageing was associated with increased body weight ($P<0.0001$) and NA contractility ($P<0.05$), reduced endothelial function ($P<0.05$), and hypertrophic remodeling ($P<0.05$; $P<0.01$). Obesogenic diet was associated with increased body weight ($P<0.0001$), reduced endothelial function ($P<0.05$), reduced MT ($P<0.001$), and structural remodeling ($P<0.05$; $P<0.01$). An age x diet interaction was observed for MT ($P<0.001$) and vascular stiffness ($P<0.001$). Fisetin treatment was associated with a reduced age-dependent difference in NA contractility, reduced endothelial dysfunction, reduced MT in young mice, and reduced structural remodeling. Rho-kinase inhibition reduced MT in the young vehicle-treated mice (both diets) and reduced MT in all Fisetin-treated mice (young/old, both diets). This is consistent with a loss of Rho-kinase activity in ageing,[1] which was partially restored by Fisetin treatment.

Overall, Fisetin treatment may have beneficial effects on aspects of the function of small arteries governing blood pressure and -flow.

C05

Menstrual endocrine fluctuations increase dynamic cerebrovascular functions

Melissa Emily Wright[1], Ian Driver[1], Cassandra Crofts[1], Saajan Davies[1], Jessica J Steventon[1], D Samuel Schwarzkopf[2], Kevin Murphy[1]

[1]Cardiff University, United Kingdom, [2]University of Auckland, New Zealand

Introduction

Recent scientific effort has started to delineate how ovarian hormones, which regularly fluctuate during the menstrual cycle, influence neural and cerebrovascular tissue. This may underlie the relationships between later hormonal decline and neurodegenerative disease risk[1]. To fully profile how hormones interact with cerebrovascular function, it is vital to consider, not just resting physiology, but also dynamic aspects of cerebrovasculature that support neural activity.

This study uses hypercapnic cerebrovascular reactivity (CVR) and visually-evoked haemodynamic response function (HRF) to investigate the influence of menstrual-related changes in oestradiol and progesterone on dynamic aspects of the cerebrovascular system.

Methods

21 menstruating females (age mean[SD]= 22.9[3.91] years) completed a 3T MRI (Siemens MAGNETOM Prisma) scanning session during the early follicular (EFP; day 1-4; N=17), late follicular (LFP; day 10-12; N=17), and mid-luteal (MLP; day 20-22; N=18) phase of their menstrual cycle (14 completed all three). All took place at the same time of day, after fasting for 4-6 hours. Circulating hormones were measured via blood samples. All procedures were compliant with ethical standards.

Simultaneous blood oxygen level dependant (BOLD)-CVR and cerebral blood flow (CBF)-CVR data were collected using a pseudocontinuous arterial spin labelling (pCASL) acquisition during periods of hypercapnia (5% CO2) with PETCO2 monitoring (maximum repetition time [TR]=3600ms, echo time [TE] 1=10ms, TE2=30ms, in-plane resolution=3.4x3.4, slice thickness=6.5mm, GRAPPA acceleration factor=3). The HRF was estimated using a whole brain EPI scan during 100% contrast checkerboard presentation (TR=2s, TE=30ms, resolution=2mm^3, multi-band acceleration factor=4).

The HRF timeseries was fit with a gamma variate model. Three metrics were extracted– peak amplitude (PA), time-to-peak (TTP), and full-width-half-max (FWHM). PETCO2 traces were used in modelling CVR maps. BOLD-CVR (Δ%BOLD/mmHgCO2) and CBF-CVR values (Δml/100g/min/mmHgCO2) were extracted across the whole brain, while HRF metrics were extracted from visually-responsive regions. Mixed linear models investigated the contribution of hormones to vascular outcomes across phases. Progesterone was regressed against oestradiol to allow investigation of independent variation (hereby called resProgesterone).

Results

Oestradiol accounted for a significant amount of global CVR variance, both for CBF-CVR ($\chi^2(1)= 50.92$; $p<0.001$; average variation attributed to oestradiol across a cycle in this sample=1.01Δml/100g/min/mmHgCO2) and for BOLD-CVR ($\chi^2(1)=59.14$; $p<0.001$; average variation attributed to oestradiol across a cycle in this sample=0.1Δ%BOLD/mmHgCO2). ResProgesterone however, was only significantly associated with global CBF-CVR ($\chi^2(1)=26.71$; $p<0.001$; average variation attributed to resProgesterone=0.6Δml/100g/min/mmHgCO2).

For HRF, increasing oestradiol was associated with slightly higher PA ($\chi^2(1)=20.55$; $p<0.001$; average variation attributed to oestradiol across a cycle in this sample=0.1%BOLD) and earlier TTP ($\chi^2(1)=10.036$; $p=0.002$; average variation attributed to oestradiol across a cycle=0.4 seconds). Increasing resProgesterone was associated with narrower FWHM ($\chi^2(1)=28.71$; $p<0.001$; average variation attributed to resProgesterone=0.5 seconds). No significant regional effects were found.

Conclusions

This study found evidence that dynamic cerebrovascular functions are associated with menstrual-related ovarian hormones. These effects were small but notable within the context of the regular menstrual cycle and raise questions about larger hormonal variations, such as within pregnancy or menopause. This may be a potential mechanism underlying menstrual symptomatology and has implications for fMRI studies that assume intact neurovascular coupling processes in women, regardless of menstrual staging, to make inferences about neural activity.

C06

Astrocyte-to-pericyte signalling underlies serotonin-mediated cerebral blood flow regulation

George Sideris-Lampretsas[1], Meiting Mai[2], David Attwell[1]

[1]University College London, United Kingdom, [2]Sun Yat-sen memorial hospital, China

Cerebral blood flow (CBF) is tightly coupled to neuronal activity. Excitatory glutamatergic activity induces local vessel dilation, while monoamines such as noradrenaline and serotonin (5-HT) stemming from brainstem neurons induce vessel constriction to maintain vascular tone. Despite its well-described role as a vasoconstrictor, the exact mechanism through which 5-HT affects blood flow remains largely understudied. Here, we show that serotonergic nerve terminals are in direct contact with capillary pericytes and astrocytic endfeet. Applying 5-HT to brain slices and in vivo induces potent pericyte constriction by activating the 5HT2C receptor, which is expressed in neurons and astrocytes. Exogenous 5-HT application induces a significant increase in the frequency, duration and amplitude of calcium transients in astrocytes and pericytes. Importantly, blocking production of 20-HETE, a potent arachidonic acid derivative that is released by astrocytes to constrict vessels, abolished the 5-HT-mediated pericyte constriction in brain slices, suggesting that 5-HT modulates pericyte contraction through astrocytes. Altogether, these data suggest that in homeostasis, 5-HT exerts its vasoactive effects on CBF by regulating astrocyte-to-pericyte communication.

In the context of Alzheimer's disease (AD), the association between serotonergic axons, pericytes and astrocytes is altered, owing to the development of markedly enlarged neuronal processes, termed axonal spheroids (AxS), that are found near Aβ plaques. AxS have been primarily studied in excitatory neurons and their development in monoaminergic and cholinergic axons remains largely unexplored. Here, we show that monoaminergic and cholinergic AxS have striking anatomical differences to glutamatergic AxS, with far greater axon swelling and distinct molecular constituents. We classify amyloid plaques based on the type of affected axons in their vicinity and explore its association with plaque compaction. Relevantly, using in vivo two-photon microscopy in anaesthetized animals expressing GRAB5-HT sensors, we show that some cortical plaques are linked to dynamic fluctuations in local 5-HT levels, possibly reflecting altered neurotransmitter release or diffusion through AxS. These findings suggest that the peri-plaque environment could be shaped by the affected axon type and raise the possibility that acetylcholinesterase inhibitors may exert their therapeutic effect by restoring peri-plaque neurotransmitter balance. We are currently investigating how the presence of cholinergic and monoaminergic AxS might influence local inflammatory responses and blood flow.

C07

Early Flow Dysregulation and Rarefaction in an Angiotensin II Infusion-Recovery Model

Declan Manning[1], Robert Cudmore[1], L. Fernando Santana[1]

[1]The University of California, Davis, United States

Loss of microvascular blood flow is a critical feature of hypoperfusion across neurovascular diseases, particularly hypertension-associated vascular dementia. However, the early mechanisms underlying capillary flow dysregulation (pre-rarefaction), stalling (functional rarefaction), and eventual microvessel loss (anatomical rarefaction), remain poorly defined and difficult to model. Here, we examine these microvascular pathologies in an Angiotensin II (AngII) infusion-recovery model in which mice receive a pressor dose of AngII (800 ng/kg/min) or vehicle saline for 28 days followed by a 14-day recovery period.

Blood pressure and heart rate were monitored by tail cuff plethysmography and microvascular flow was quantified at two-week intervals through an acute cranial window using two-photon line scan imaging and Radon transform analysis. Flow velocity, temporal variability and stall frequency were assessed in the first four capillary branch orders adjoining precapillary arterioles. Brains were subsequently collected for immunohistochemical analyses of endothelial cells, pericytes and tissue hypoxia.

AngII induced severe hypertension by week two (131±4 mmHg AngII vs. 100±3 mmHg saline; N=8 vs. N=8; p=0.0002) which persisted through week four (136±3 mmHg AngII vs. 111±3 mmHg saline; N=8 vs. N=8; p=0.0002) and normalized by week six (105±4 mmHg AngII vs. 101±3 mmHg saline; N=8 vs. N=8; p=0.8706). Capillary flow velocity slowed considerably by week four (0.79±0.07 mm/s AngII vs. 1.13±0.09 mm/s saline; N=4 vs. N=5; p=0.0125) and remained reduced at week six (0.87±0.06 mm/s AngII vs. 1.18±0.10 mm/s saline; N=6 vs. N=6; p=0.0389) despite normalized blood pressure. Flow variability, measured as temporal coefficient of variation (CV) excluding stalls, was unchanged during infusion but increased at recovery week six (AngII CV=0.28±0.02, saline CV=0.18±0.01; N=6 vs. N=6; p=0.0021). Stalling rose progressively, peaking at recovery week six (AngII 24.2±2.6% vs. saline 9.9±1.9%; N=6 vs. N=6; p<0.0001).

These functional disturbances were accompanied by anatomical rarefaction. Microvessel loss was pronounced in the hippocampus of six-week AngII recovery mice (5.9±0.4% AngII vs. 8.2±0.4% saline CD31+ vessel density; N=6 vs. N=6; p=0.0005) with concurrent pericyte loss (2.1±0.3% AngII vs. 3.8±0.2% AngII PDGFRb+ pericyte density; N=6 vs. N=6; p=0.0002). This coincided with substantial tissue hypoxia (17.0±0.8% AngII vs. 0.9±0.1% saline HypoxyProbe+ tissue area; N=6 vs. N=6; p<0.0001). By contrast, the cortex displayed a trend towards microvessel loss (9.2±0.3% AngII vs. 10.0±0.4% saline CD31+ vessel density; N=6 vs. N=6; p=0.2528), significant pericyte loss (2.6±0.3% AngII vs. 4.5±0.3% saline PDGFRb+ pericyte density; N=6 vs. N=6; p<0.0001) and less pronounced hypoxia than the hippocampus (4.1±0.8% AngII vs. 0.7±0.1% saline HypoxyProbe+ tissue area; N=6 vs. N=6; p=0.0009).

Together, these findings show that four-week AngII infusion initiates early microvascular rarefaction, producing persistent microvessel loss even after a two-week return to normotension. The hippocampus exhibits the greatest anatomical vulnerability, whilst the cortex shows marked flow dysregulation and stalling consistent with early-stage rarefaction. These early disturbances likely precede broader neurological consequences observed in extended AngII models. This preliminary data outlines the early steps linking hypertension to hypoperfusion, regional hypoxia, and cognitive decline, laying the groundwork for future efforts to define the mechanisms driving microvascular rarefaction in vascular dementia.

C08

Amyloid-β driven neuronal hyperexcitability creates energy imbalance in an Alzheimer's mouse model, particularly affecting the hippocampus

Harry Trewhitt[1], Kira Shaw[2], Silvia Anderle[3], Letitia McMullan[1], AlBeshr Almasri[1], Catherine Hall[1]

[1]University of Sussex, United Kingdom, [2]University of Manchester, United Kingdom, [3]University College London, United Kingdom

Introduction

Active neurons dilate nearby blood vessels, ensuring sufficient oxygen availability, fuelling this activity. Neurovascular coupling (NVC) mechanisms facilitating this functional hyperaemia may be disrupted early in Alzheimer's Disease (AD) pathogenesis through direct actions of Beta-Amyloid (Aβ) on neurovasculature and/or induction of chronic neuronal hyperexcitability, impairing the ability of healthy NVC to be sustained. The hippocampus is affected early in AD which may be partly driven by its lower vascularisation and NVC response compared to cortex, making it particularly vulnerable to further NVC disruption. APOE4, the strongest risk allele for sporadic AD, may also confer compromised NVC in carriers, and is an integral link between systemic cardiovascular health and AD.

Aims

In the current study we aim to unpick contributions of Aβ accumulation and APOE genotype to early-AD NVC impairment, comparing the hippocampus to the visual cortex.

Methods

To do this we have employed a novel mouse model combining humanised APOE (3/3 or 4/4) and doxycycline-inducible APPSwe/Ind transgenes, as well as the CaMKII driven GCaMP6f neuronal calcium indicator. By measuring, *in vivo,* brain blood flow and oxygenation, neuronal activity, and vascular dilatory responses, before and after induction of Aβ expression we aim to untangle the relative impact of low level Aβ on different aspects of neurovascular physiology, and to understand how these changes could feed into gradual neurodegeneration.

Statistical Analyses

Data were analysed using linear mixed models to determine the effects of genotype, time off doxycycline and brain region, with animal ID specified as the random factor (n=7-18 mice per condition).

Ethics

All experimental procedures were approved by the UK Home Office, in accordance with the 1986 Animal (Scientific Procedures) Act, and the University of Sussex animal welfare ethical review board.

Results

Preliminary data suggests that soluble but not aggregated Aβ increases in both cortex hippocampus over 3 months, causing cortical neurons to become hyperexcitable. Over the same timescale, cortical blood flow increases from baseline, possibly to counter this hyperexcitability, but decreases in the

hippocampus. However, blood oxygenation decreases in both the cortex and hippocampus, suggesting any increase in blood flow is insufficient to counter increased oxygen consumption by neurons.

Conclusions & Future Directions

Ongoing analyses will interrogate influences of APOE genotype, characterise any effect on hippocampal neurons and cortical and hippocampal NVC.

C09

Systemic inhibition of nitric oxide synthesis alters vascular tone, vasomotion and brain oxygen availability and reduces network-level coordination of cerebrovascular physiology

Catherine Hall[1], Letitia McMullan[1]

[1]University of Sussex and University College London, United Kingdom

Nitric oxide (NO) is a critical regulator of vascular tone and cerebral blood flow, and reduced NO bioavailability is implicated in both cardiovascular and neurodegenerative disease. Although inhibition of nitric oxide synthase (NOS) is known to alter cerebral haemodynamics and vasomotion, its effects are typically assessed using individual physiological measures in isolation. Here, we applied a multivariate systems-level approach to characterise how NOS inhibition reshapes coordinated cerebrovascular and systemic physiology.

Multiple indices of systemic and cerebrovascular function were recorded simultaneously in awake mice under control conditions and following administration of the non-specific NOS inhibitor L-NG-nitroarginine methyl ester (L-NAME; 75 mg kg^{-1}, s.c.). Cerebral blood flow, blood oxygenation, total haemoglobin and derived oxygen metabolism ($CMRO_2$) were measured in visual cortex and hippocampus alongside peripheral heart rate, respiratory rate, arterial oxygen saturation, pulse distension and blood pressure. Vasomotion and neurovascular coupling were quantified from these signals.

L-NAME reduced heart and respiratory rates and increased blood pressure, with minimal effects on peripheral oxygen saturation. In contrast, cerebral blood flow, oxygenation and $CMRO_2$ were markedly reduced in both regions, while blood volume was relatively preserved. Vasomotion power and frequency increased substantially, particularly in the hippocampus, whereas microvascular pulsatility increased similarly across regions and neurovascular coupling remained largely intact. Multivariate analyses combining principal component analysis with mixed-effects modelling revealed dissociable physiological axes reflecting direct effects of NOS inhibition and secondary effects mediated by reduced cerebral oxygenation. Notably, changes in vasomotion were more strongly associated with reductions in cerebral oxygenation than with drug condition itself, indicating that some effects commonly attributed to loss of NO signalling may instead arise from secondary hypoxia. These findings suggest that NOS inhibition produces complex cerebrovascular changes that cannot be assumed to reflect direct NO-dependent mechanisms alone.

C10

How does a mild decrease in brain oxygen supply constrain hippocampal function?

Letitia McMullan[1], Melissa Scholefield[2], Harry Trewhitt[1], Magali Ostroviecki[1], Catherine Hall[1]

[1]University of Sussex, United Kingdom, [2]University of Manchester, United Kingdom

Introduction

Baseline blood flow (CBF), blood oxygen saturation (sO2), and vascular density are lower in the hippocampus than the visual cortex (V1), despite similar oxygen consumption rates. The hippocampus is therefore predicted to exist at a watershed whereby neurons furthest from the blood vessels only just receive enough oxygen to function properly in a normal healthy brain. Consequently, the hippocampus is likely to be especially vulnerable to even mild decreases in brain blood or oxygen supply, as seen in Alzheimer's disease (AD) and acute mountain sickness (AMS), for example.

Aims

Our aim was therefore to determine if a mild decrease in brain oxygen supply differently affects function in hippocampus compared to neocortex (V1).

Methods

To achieve this, we mildly reduced the fraction of inspired oxygen (FiO2) using an altitude generator. The generator supplied mice with air of 21-11% FiO2 via a nose cone or tent enclosing the mouse's cage. In awake head-fixed mice that previously underwent surgery to place a cranial window over the hippocampus or neocortex, we recorded haemodynamic changes using a combined laser-doppler flowmetry haemoglobin spectroscopy (oxy-CBF) probe, and neuronal calcium signalling using 2-photon microscopy. We also performed biochemical assays and mass spectrometry to measure the effects of hypoxia on metabolism and nutrient homeostasis in post-mortem brain tissue collected from mice exposed to 1hr at 21% or 11% FiO2.

Statistical Analyses

Robust linear mixed models assessed effects of FiO2, brain region and their interaction, with animal ID as the random factor (n=4-9 mice per condition).

Ethics

All experimental procedures involving animals were approved by the UK Home Office in accordance with the 1986 Animals in Scientific Procedures Act, as well as by the University of Sussex animal welfare ethical review board.

Results

Baseline CBF and sO2 were lower in hippocampus than neocortex. Mild hypoxia briefly increased CBF but decreased sO2 more in hippocampus than in neocortex. This caused hippocampal pyramidal cells to fire more frequently but with less synchronisation and coordination within and between neurons. Conversely, neocortical pyramidal neurons fired less frequently but synchronisation and coordination

were preserved. The increased frequency of neuronal calcium events in hippocampal pyramidal cells likely resulted from disinhibition since the frequency of neuronal calcium events decreased in hippocampal inhibitory interneurons. Neurovascular coupling was preserved in both regions. Mild hypoxia reduced iron levels in the hippocampus but not in neocortex.

Conclusions

Overall, mild decreases in brain oxygen supply produce lower oxygenation in hippocampus than neocortex. This causes different effects on neuronal activity and nutrient homeostasis and may help explain why the hippocampus is one of the most affected regions in AD and AMS.

Future Directions

Existing data are being extracted to determine whether hypoxia-sensitive TRPA1 channels may be responsible for neuronal calcium signalling changes in hippocampus. Current experiments are testing the effects of more chronic (2 week) mild hypoxia exposure on hippocampal neuronal and vascular function and amyloid beta accumulation a mouse model of AD.

C11

Characterising the Effect of NLRP3 Inflammasome-Induced Vascular Neuroinflammation on Blood Brain Barrier Integrity

Alexander Brenchley Williams[1], Joern R. Steinert[1], Michael T. Heneka[2]

[1]University of Nottingham, United Kingdom, [2]Luxembourg Centre for Systems Biomedicine, Luxembourg

Various studies have implicated neuroinflammatory NLRP3 inflammasome activation in a host of neurodegenerative diseases with neurovascular aspects, though the interaction between the inflammasome and the blood-brain barrier has yet to be deciphered. This project aims to assess the effect of NLRP3 inflammasome activation on the integrity of the neural endothelium, independent of cell death, and investigate the underlying pathways. Furthermore, this project aimed to elucidate the electrophysiological effects of endothelial TLR4 activation by LPS, with potassium efflux being a key regulator of NLRP3 inflammasome activation.

hCMEC/D3 cells were cultured in EGM-2 Basal Medium and SingleQuots supplements 5% foetal bovine serum, 0.4% human fibroblast growth factor-B, 0.04% hydrocortisone and 0.1% ascorbic acid along with 1% Pen-Strep. LPS treatments were conducted over 6 hours, or 5 hours + hour 10μM nigericin with or without an hour of 20μM MCC950 treatment. Permeability assays were conducted on endothelial monolayers cultured on 0.4μm Transwell membranes, followed by ion permeability assessment by a Voltohmeter, and 2000kDa Dextran-Fluorescein flow determined by ID3 Spectramax plate reader. Protein for western blotting was obtained by scraping with RIPA buffer and membranes were read using a LICOR ODESSEY. Immunofluorescence was imaged using a Zeiss AxioObserver7 confocal microscope and analysed by ImageJ.

Whole-cell currents were recorded using a MultiClamp 700B amplifier for data acquisition (n=6-10 cells per condition) and analysis was performed with Clampex 11.2 (Molecular Devices) software. Whole-cell currents were recorded in HEPES buffered standard solution at a perfusion rate of 4ml/min and ~35ºC.

All graphed data is presented as mean ± SEM. Statistical analysis was performed using GraphPad Prism 10 software and used one- or two-way ANOVA followed by Tukey's multiple comparisons, or unpaired t-tests. Significance was set at *p < 0.05.

Following treatment, Dextran permeability increased by $5.89\times10^{-12}\pm1.513\times10^{-12}$ mol/cm^2×S (p=0.0078) and TEER decreased by 42.68±7.944% (p=0.0003) in comparison to the healthy controls. MCC950 prior to nigericin addition showed a 36.97±10.26 % increase (p=0.013) in ion permeability compared with the LPS + nigericin treated groups (n=3-7 independent experiments). Western blotting confirmed inflammasome activation and immunofluorescence showed inflammasome localisation, a shift in morphology and a reduction of tight and adherens junction localisation to the cell membranes in NLRP3 inflammasome activated cells (3 replicates). Interestingly, LPS treatment reduced whole-cell currents at 50mV by -100.2±31.37pA (p=0.0085, N=6-7) compared with untreated cells and $V^{1}/^{2}$ K^+ by 10.99±4.302mV (p=0.0268, N=6-7).

These findings imply that NLRP3 activation is disruptive to the BBB by altering the morphology and junction protein expression of microvasculature endothelial cells, though further research is needed to decipher the underlying pathways involved. The effect of NLRP3 inflammasome inhibitor MCC950 in reversing some of these effects could show some future therapeutic potential for rescuing inflammatory-associated vascular dysfunction in AD in conjunction with anti-amyloid treatments. The

electrophysiology studies show a novel effect of TLR4 activation that may influence K^+ efflux for inflammasome activation.

C12

Acute Microvascular Effects of Cilostazol and Isosorbide Mononitrate Reveal Regional Redistribution of Cerebral Blood Supply in Wild-Type Mice

ALBESHR ALMASRI[1], Harry Trewhitt[1], Letitia McMullan,[1], Catherine Hall[1]

[1]Brain Energy Lab, Sussex Neuroscience, School of Psychology, University of Sussex, United Kingdom

Background:

White matter (WM) is preferentially damaged in cerebral small vessel disease (cSVD), likely due to its susceptibility to chronic hypoperfusion (Wardlaw et al., 2013). Cilostazol (CIL) and isosorbide mononitrate (ISMN) have been shown in clinical LACI trials to improve memory and reduce stroke risk (Wardlaw et al., 2023); however, the acute cerebrovascular mechanisms and the vascular compartments at which these drugs act remain unclear. We investigated whether CIL and ISMN induce age- and region-dependent acute changes in microvascular haemodynamics.

Methods:

Wild-type C57BL/6J mice of both sexes underwent cranial window implantation at approximately 12 weeks of age over WM or cortical grey matter (GM). For WM windows, ~800 µm of cortex was aspirated over the corpus callosum and a custom 3D-printed window with a glass base was implanted. GM windows were placed over the visual cortex without aspiration, preserving pial arteries. Mice were first recorded at 4 months of age; the same WM mice were re-recorded after 8 months of ageing (1 year old).

Using a blinded crossover design, mice received vehicle or combined CIL+ISMN with ≥6-day washout. Haemodynamics were recorded at baseline, 30 min, 1 h, 2 h, 4 h, 6 h, and 24 h using combined laser Doppler flowmetry and haemoglobin spectroscopy. Measures included red blood cell (RBC) flux, RBC speed, concentration of moving RBCs, oxygen saturation (sO_2), total haemoglobin (HbT), and derived cerebral metabolic rate of oxygen ($CMRO_2$). Awake, head-fixed recordings were obtained during resting periods. Linear mixed-effects models were used with drug and timepoint as fixed effects and animal ID as a random effect, with Dunnett post-hoc tests. Drug doses were scaled from the LACI-2 trial using body-surface-area conversion.

Results:

In deep tissue containing WM of young mice (n = 8), CIL+ISMN significantly reduced RBC flux (treatment effect $p = 0.022$; timepoint × treatment $p = 0.032$), driven by a marked reduction at 6 h (estimate −0.22 ± 0.06, $p = 0.0003$). RBC concentration was also reduced ($p = 0.0072$), while RBC speed was unchanged. $CMRO_2$ decreased significantly ($p = 0.016$), most prominently at 6 h ($p = 0.0007$), without significant changes in sO_2.

In the same mice re-examined longitudinally after 8 months of ageing (n = 4), WM responses to CIL+ISMN were preserved, with significant reductions in RBC flux ($p = 0.013$), RBC concentration ($p = 0.041$), and $CMRO_2$ ($p = 0.007$).

In contrast, GM showed a significant increase in moving RBC concentration ($p = 0.003$), a modest reduction in HbT ($p = 0.044$), and a trend toward increased sO_2 ($p = 0.082$), with no change in flux or speed. Blood pressure under sedation did not differ between baseline, vehicle, or drug conditions.

Conclusions:

Our data indicate region-specific microvascular responses to cilostazol and isosorbide mononitrate, with preserved cortical grey matter microcirculation and reduced red blood cell delivery and oxygen consumption in deep tissue containing white matter. These findings support an acute redistribution of microvascular resources rather than a uniform microvascular response. Ongoing two-photon imaging and chronic hypoperfusion models will determine the vascular origin and pathological relevance of this redistribution under chronic treatment conditions.

C13

Blood-brain barrier permeability during ageing in rodent models – a systematic review and meta-analysis

Mitchell Hudson[1], Claire L Gibson[2]

[1]School of Psychology, University of Nottingham, Unitedd Kingdom, [2]School of Psychology, University of Nottingham, United Kingdom

Ageing is known to impact the cerebral vasculature and impacts nutrient delivery, waste clearance and the regulatory functions of the blood-brain barrier (BBB). Evidence indicates that the BBB undergoes measurable changes during healthy or normal ageing, even in the absence of overt neurodegenerative disease (Cummins et al., 2024). Mapping these changes across the lifespan is essential for understanding the biology of healthy brain ageing and for identifying early biomarkers of vulnerability. Rodent models remain central to experimental studies of the BBB in ageing, and brain ageing in general. Observations of increased permeability in aged animals and humans are common, but the magnitude, time of onset, species or sex-effects and regional specificity of these changes vary widely between studies. The present systematic review and meta-analysis aims to quantify age-associated changes in BBB permeability (integrity failure/ loss of selective permeability/ increase in permeability rate), in healthy and modified ageing rodent models, and across multiple tracer types, species and sex. This will allow us to assess heterogeneity in effect sizes attributable to methodological and biological moderators, including tracer properties, detection method, (brain region, species, strain,) and age definition. This systematic review and meta-analysis were conducted in accordance with the Preferred Reporting Items for Systematic Reviews and Meta-Analyses (PRISMA) 2020 statement (Page et al., 2021). Inclusion and exclusion criteria were determined and appropriate literature searches conducted from which data including PS/PA (permeability–surface area product), K_trans (DCE-MRI), Tex (water exchange time from ASL MRI), tracer Ki (unidirectional transfer constant), Evans blue–albumin extravasation and endogenous IgG or albumin leakage was collected. Overall, we identified 14 for studies meeting the inclusion criteria for quantitative effect size analysis which included 8 studies reporting BBB permeability dysfunction and 6 studies reporting BBB permeability transport changes. Aged mice (typically ~18–30 months), tended to have higher rates of permeability, as well as showing higher levels of large molecule extravasation across the BBB when compared to younger controls (typically ~2–4 months), based on data using a variety of tracer methods including, but not limited to; PS/PA of Sucrose C14, Ktrans DCE-MRI, Evans blue dye, endogenous IgG, and albumin/IgG-depleted signal. Further analysis will determine the efficacy of different tracing methods and compare changes in BBB permeability according to species, strain (where possible), sex, tracer method and comparing healthy ageing with modified ageing models. Age-related BBB permeability increases may contribute to neuroinflammation, neuronal stress and cognitive decline. However, it is important to assess, the comparability of using healthy aged animals with modified ageing models and understand changes according to sex, species and methodological approach. Healthy ageing models require substantial investment in terms of resources, both time and financial whereas modified ageing models, if similar changes in BBB permeability are seen, can offer a more efficient route to experimental data. Additionally, it is important to consider sex-specific effects and the efficacy across a variety of tracers to determine the optimal experimental designs for exploring mechanistic changes in BBB permeability and function.

C14

Targeting the Blood-Brain Barrier: New Frontiers in Neurodegeneration and Brain Health

Mootaz Salman[1]

[1]University of Oxford, United Kingdom

Neurodegenerative diseases are multifactorial and heterogeneous conditions and leading cause of morbidity and mortality. Our work aims to answer the question: how does inflammation-mediated blood-brain barrier (BBB) dysfunction lead to the development of neurodegeneration and whether we can stop it? Increasing evidence supports the involvement of BBB dysfunction in neurodegenerative disorders including Parkinson's, Alzheimer's and small vessel dementia; it is evident that this dysfunction happens even before the onset of dementia. In-depth understanding of the cell-cell interactions and signalling pathways between the core elements of the BBB will help in defining and validating new therapeutic targets for the prevention of dementia.

In our work, we developed advanced microfluidic 3D BBB-on-a-chip models using patient-derived iPSCs and human primary cells and identified a number of molecular targets that contribute to barrier integrity and function in astrocytes and pericytes. Our work provides new tools to understand lifelong brain health, describe the basis of BBB dysfunction in the occurrence and development of neurodegeneration, and provides a platform to develop new treatments for dementia and related CNS pathologies.

C15

Hypercapnia, a potential biomarker for vascular dementia, elicits increased cortical cerebral blood flow through connexin channels.

Shereen Nizari[1], Shefeeq Theparambil[2], Anna Hadjihambi[3], Patrick Hosford[4], Sofia Nur Nizar[1], Charith Perera[1], Mark Lythgoe[1], Ian F Harrison[1], Jack A Wells[1], Alex Gourine[4]

[1]Centre for advanced biomedical imaging, University College London, UK, [2]Biomedical and Life Sciences, Lancaster University, UK, [3]The Roger Williams Institute of Hepatology, UK, [4]Centre for cardiovascular and metabolic neuroscience, University College London, UK

Introduction:

The human brain produces a staggering 75 litres of CO2/day. We recently published data demonstrating CO2 mediates neurovascular coupling, affecting cerebral blood flow (CBF) (Hosford *et al.*, 2022). A meta-analysis published by our group suggested that nitric oxide and cyclooxygenase (COX) are key modulators of this response (Hosford *et al.*, 2022). However, the mechanisms behind this phenomenon and the implications for cerebrovascular disease remain incompletely understood.

Aims

In this study, we aim to characterise the molecular mechanism behind hypercapnia induced vasodilation of the cerebrovasculature. We also aim to characterise this effect on cerebrovascular reactivity in the hyperhomocysteinemia (HHcy) mouse model of vascular dementia.

Methods

Vessel diameter changes in cortical arterioles were recorded from ex vivo rat brain slices, pre-constricted with L-phenylephrine (200μM) in artificial cerebral-spinal-fluid (aCSF). Isohydric hypercapnia (pH 7.35) was induced by bubbling aCSF with 13.5% CO2 containing 80mM sodium bicarbonate. Ex vivo and in vivo dye loading experiments were carried out on brain slices and open cranial windows on 10-week-old male C57BL6 mice using aCSF containing 200μM carboxyfluorescein. Hypercapnia in in vivo studies was delivered by free-breathing of 10% CO2. The diet-induced HHcy model of vascular dementia, known to develop cognitive impairment and cerebral microbleeds (Sudduth *et al.*, 2013), was carried out on C57BL6 mice of both sexes (n=20). CBF and cerebrovascular reactivity to hypercapnia were quantified using arterial-spin-labelling MRI (9.4T Bruker) under medetomidine/isoflurane anaesthesia.

Results

Recording of cortical arteriolar diameter changes in these slices confirmed CO2 induced vasodilation independent of CO2 induced acidification ($p<0.05$, n=9, t-test). Vasodilation was prevented by COX-1 inhibition ($p<0.001$, n=6, one-way-ANOVA) and was affected by neuronal nitric oxide synthase (NOS) inhibition ($p<0.001$, n=6, one-way-ANOVA), but not endothelial NOS inhibition ($p>0.05$, n=6, one-way-ANOVA) or neuronal activity inhibition (TTX) ($p>0.05$, n=6, one-way-ANOVA). Additionally, we found that

hypercapnia-induced dilation depends on purinergic signalling (n=6) and is modulated by connexin/pannexin channel availability ($p<0.01$, n=6, one-way-ANOVA). We confirmed the role of these channels through loading of carboxyfluorescein, a connexin/pannexin channel permeable dye. Concentration dependent CO_2 ex vivo dye loading in brain slices was blocked by connexin channel inhibitors. This was confirmed in vivo in the mouse somatosensory cortex, using hypercapnia ($p<0.01$, n=5, one-way-ANOVA), and CO_2 release induced by forepaw stimulation ($p<0.01$, n=5, one-way-ANOVA).

In the HHcy model of vascular dementia, no differences in basal CBF or cognitive impairment were detected after 10 weeks on the HHcy inducing diet. However, cerebrovascular reactivity to hypercapnia was significantly reduced in mice on the HHcy diet compared to those on the control diet ($p<0.05$, n=20, t-test). This is suggestive of early disrupted cerebrovascular reactivity, a translational biomarker which could precede cognitive deficits and changes to basal perfusion.

Conclusion

In conclusion, our studies indicate that hypercapnia-induced cerebrovascular dilation is dependent upon neuronal nitric oxide release, purinergic signalling, and CO_2 induced connexin channel availability. Further studies are underway to understand the mechanisms driving the impairment of cerebrovascular reactivity to hypercapnia in the HHcy mouse model, highlighting its potential to be used as a much-needed early biomarker of vascular dementia.

C16

Advanced MRI shows subtype-specific vascular characteristics in Gliomas

Eleonora Patitucci[1], Stefano Zappalà[2], James Powell[3], Najmus Sahar Iqbal[3], Richard Wise[4], Michael Germuska[5]

[1]CUBRIC, School of Psychology, Cardiff University , United Kingdom , [2]CUBRIC, School of Computer Science and Informatics, Cardiff University, United Kingdom , [3]Department of Oncology, Velindre University NHS Trust, Cardiff, United Kingdom, [4]Department of Neurosciences, Imaging, and Clinical Sciences, University 'G. D'Annunzio' of Chieti-Pescara, Chieti, Italy, [5]Department of Radiology, University of California Davis Medical Center, Sacramento, California, United States

INTRODUCTION
Gliomas generate an additional blood supply to meet their increased need for nutrients and oxygen, altering normal physiology and tissue metabolism[1,2]. As proliferating cells demand more blood flow, the structure and function of the brain's vasculature are disrupted. Vascular proliferation is a pathological hallmark of gliomas, leading to abnormal and dysfunctional vessels[3]. Considerable heterogeneity exists within tumours regarding vascular morphology. For example, high microvessel density is characteristic of astrocytic gliomas, and high-grade tumours exhibit pronounced neovascularization[4].

The formation of new blood vessels to support tumour growth has clinical consequences, most notably the development of vasogenic edema, this can lead to an increase in intracranial pressure due to leakage of the blood–brain barrier[5].

AIM
This study used advanced MRI techniques to characterize vascular differences across glioma subtypes.

METHODS
The study was approved by the NHS Research Ethics Committee, Wales, UK and Cardiff University's Ethics Committee, School of Psychology, Cardiff, UK.

Quantitative susceptibility maps (QSM) were acquired from 27 patients (mean age 45.5 ± 8.8 years; 20 male) diagnosed with glioma. Vascular parameters—including vessel density, vessel diameter, and oxygen extraction fraction (OEF)—were extracted from the QSM maps.
Pre- and post-contrast T1-weighted images (gadolinium-enhanced), T2-weighted images, and T2-FLAIR were used to segment brain tissue into tumour core (enhancing vs. non-enhancing), edema, necrotic area, cavity, and residual healthy grey matter. (**Figure 1**)

ANOVAs were conducted to evaluate differences in OEF (within skeletonized vessels), vessel diameter, and vascular density in edema, tumour core, and residual healthy grey matter. Gender was included as a covariate.

RESULTS

Structurally, we observed increased vessel diameter in edema and tumour core regions compared with residual healthy grey matter ($F(2,38) = 11.08$; $p < 0.01$) (**Figure 2-A**). Vascular density was higher in enhancing tumour tissue compared with non-enhancing tumour regions and healthy grey matter ($F(2,38) = 16.81$; $p < 0.01$). (**Figure 2-B**)

Physiologically, OEF was reduced in non-enhancing tumour regions compared with healthy grey matter and enhancing tumour tissue. This result may reflect infiltration or hypoxia, with altered OEF and modest vascular changes consistent with metabolic stress or tissue loss ($F(2,38) = 7.16$; $p < 0.01$) (**Figure 2-C**).

Cerebral blood flow (CBF) was reduced in both enhancing and non-enhancing tumour areas compared with healthy grey matter, indicating vascular–metabolic decoupling in enhancing cores likely related to abnormal vessel structure and shunting ($F(2,38) = 22.07$; $p < 0.01$) (**Figure 2-D**).

CONCLUSION

Our findings demonstrate the potential of QSM to identify distinct metabolic and vascular characteristics across glioma subtypes, consistent with evidence that more aggressive tumours develop their own blood supply, leading to altered vascular parameters.

Integrating QSM into routine glioma assessment may enable non-invasive hypoxia evaluation, differentiation from non-tumour abnormalities, and support individualized treatment planning. This approach could help guide surgical and radiotherapy strategies and facilitate longitudinal monitoring of treatment response.

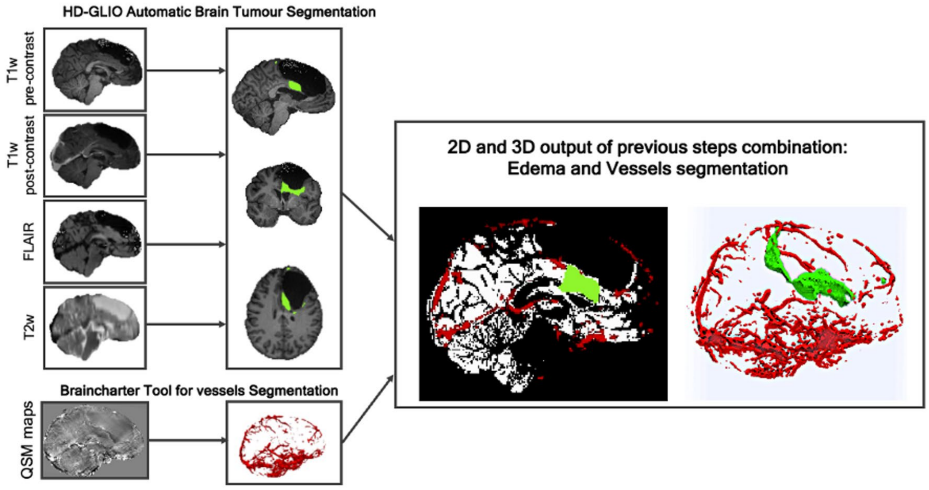

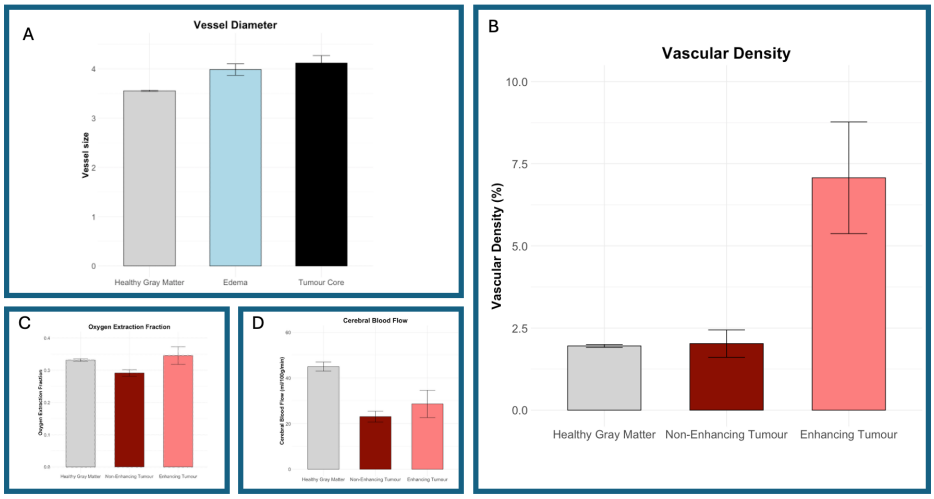
A
Vessel Diameter
Vessel size
Healthy Gray Matter
Edema
Tumour Core
B
Vascular Density
Vascular Density (%)
10.0
7.5
5.0
2.5
0.0
Healthy Gray Matter
Non-Enhancing Tumour
Enhancing Tumour
C
Oxygen Extraction Fraction
D
Cerebral Blood Flow

C17

Long Non-coding RNA Signatures Mediate Microvascular Maladaptation from Pregnancy-induced to Chronic Hypertension

Maizura Mohd Zainudin[1], Prianeesha Ganesan[1], Hidayatul Radziah Ismawi[1], Khodijah Zulkiflee[1]

[1]International Islamic University Malaysia, Malaysia

Background: Hypertension remains a major global health burden and a leading cause of cardiovascular morbidity and mortality. Approximately 10% of pregnancies are complicated by hypertensive disorders such as pregnancy-induced hypertension (PIH) and pre-eclampsia. These conditions not only contribute to adverse perinatal outcomes but also predispose women to persistent endothelial dysfunction (ED) and a higher lifetime risk of cardiovascular disease (CVD). PIH is defined as a transient elevation in blood pressure (≥140/90 mmHg) occurring after 20 weeks of gestation in previously normotensive women, without proteinuria or other systemic involvement. It typically resolves after delivery, suggesting a reversible endothelial disturbance. In contrast, chronic hypertension, represented by the spontaneously hypertensive rat (SHR) model, is characterised by sustained, non-pregnancy-related hypertension associated with vascular remodelling, increased arterial stiffness, and irreversible endothelial injury. Understanding the molecular differences between these conditions is crucial to elucidate why some women with PIH women subsequently develop chronic hypertension and CVD earlier in life. **Objective:** This study aims to characterise long non-coding RNA (lncRNA)-mediated transcriptomic signatures underlying transient (PIH)and chronic (SHR) forms of endothelial dysfunction. **Methods:** Three rat groups (Control, PIH, and SHR; n = 6 per group) were included in the study. Blood pressure was recorded at gestational day 13, day 19, and postpartum days 7 and 30. Aortic and mesenteric arteries were harvested for RNA sequencing using the DNBSEQ G400RS platform. Differential gene expression, principal component analysis (PCA), correlation heatmaps, and Venn diagram analyses were performed to compare transcriptomic profiles. **Results:** PIH rats exhibited a transient increase in mean arterial pressure at gestational day 19, which normalised postpartum, whereas SHR maintained persistently elevated blood pressure. A total of 348, 597, and 337 differentially expressed genes (DEGs) were identified in PIH vs Healthy, SHR vs Healthy, and PIH vs SHR, respectively, with 83 shared DEGs. PCA demonstrated clear separation of SHR samples, consistent with chronic endothelial injury, whereas PIH clustered near controls, indicating reversibility. Heatmap and Venn analyses revealed distinct lncRNA expression patterns, with SHR showing greater transcriptomic divergence. **Conclusion:** PIH and chronic hypertension exhibit distinct molecular programs of endothelial dysfunction. lncRNA-driven regulatory networks appear central to microvascular adaptation and maladaptation, providing novel insights into post-pregnancy cardiovascular risk and potential lncRNA-targeted therapeutic strategies.

C18

Physiological oxygen levels reset K+ channel activity in human vascular endothelial cells

Fan Yang[1], Giovanni Mann[2], Joern Steinert[3]

[1]King's College London, United Kingdom, [2]King's College London, United Kingdom, [3]University of Nottingham, United Kingdom

Human vascular endothelial cells play a critical role in vascular homeostasis and their function is influenced by oxygen tension, which varies in a spatial-temporal manner across tissues (Keeley & Mann, Physiol. Rev. 99:161-2340. This study investigates the effects of adapting human brain microvascular endothelial cells (hCMEC/D3) to physiological oxygen tension (5kPa O2) on their basal potassium (K^+) channel activity, as well as agonist- induced whole-cell K^+ currents. Our data show that hCMEC/D3 exhibited only outwardly rectifying K^+ currents. Compared to standard culture under 18 kPa O2, long-term adaptation of hCMEC/D3 to 5 kPa O2 exhibited larger outward currents under basal (+60mV: 0.598±0.058nA) and NO-stimulated whole-cell K^+ currents (+60mV: 0.795±0.0.075nA), measured at –20mV and +60mV holding potentials using Nanion Port-a-Patch apparatus maintained in an oxygen-controlled Scitive dual workstation (Baker, USA). Acute application of a NO donor (NOC-7, 400mM) increased outward currents only under 5kPa (40mV: P=0.0053 and 60mV: P<0.0001, two-way ANOVA). However, under 18kPa O2, NO did not induce a current potentiation at any holding voltage (two-way ANOVA). To examine the effects of sequentially blocking BK, IK and SK channels, different K+ currents were pharmacologically isolated using tetraethylammonium (TEA, 10mM), TRAM-34 (5μM) and apamin (100nM) revealed differential effects in cells adapted to 5kPa or 18kPa O2. Under 5kPa O2 cells also exhibited a larger proportion of currents sensitive to all blockers (82%) compared to 44% in hyperoxic cultures. At 5kPa O2, each inhibitor caused a significant reduction in whole-cell current amplitudes at 50mV relative to basal control currents (data expressed as normalised current relative to maximal amplitude at 50mV, 5kPa and 18kPa: TEA: 58±9% P=0.0291 and 74±7% P=0.2394, TEA+TRAM-34: 37±2% P=0.0011 and 65±14% P=0.0743, TEA+TRAM-34+apamin: 18±2% P<0.0001 and 56±12, P=0.0193, n=3 each, two-way ANOVA). Changes in pericellular O2 levels had negligible effects on protein expression and fluorescence intensity of KCa1.1, KCa3.1 and KCa2.3 channels, suggesting that changes in whole-cell currents in were due to channel modulation. Thus, our findings reveal that physiological O2 tension shapes the electrophysiological phenotype of human EC by modulating K^+ channel function and NO responsiveness. The novel insights into the modulation of EC K^+ channels by O2 has implications for the regulation of vascular tone and design and use of experimental models *in vitro* for high throughput drug discovery and clinical translation.

C19

Physiological oxygen levels determine ion channel activities: characterising the role of physoxia in neuronal function

Jenifer Cale[1], Sébastien Serres[1], Tracy Farr[2], Joern R Steinert[1]

[1]University of Nottingham, United Kingdom, [2]University of Edinburgh, United Kingdom

Physiological oxygen levels determine ion channel activities: characterising the role of physoxia in neuronal function

Jennifer Cale[1], Sébastien Serres[1], Tracy D. Farr[2] and Joern R. Steinert[1]

[1]School of Life Sciences, University of Nottingham, NG7 2UH, UK

[2]Institute for Neuroscience and Cardiovascular Research, University of Edinburgh, Queen's Medical Research Institute, EH16 4TJ

Introduction and aims:

Vascular dementia caused by vascular dysfunction is the second most common type of dementia after Alzheimer's disease and it is associated with hypoxia; oxygen supply drops below physiological levels of about 5kPa to less than ~2kPa. Mechanistic studies are often carried out under hyperoxic (21kPa) conditions. We sought to characterise neurophysiological regulation at different oxygenation concentrations to addresses this gap by examining ion channel behavior under physioxia (5kPa) to reflect physiological environments. We cultured differentiated mouse-derived neuroblastoma cells for 4 days under physiological or hyperxoxic (21kPa) conditions as well as for 1 day under hypoxic O2 (1kPa) conditions.

Methods:

Mouse neuroblastoma cells (N2a) were cultured in DMEM+GlutaMAX media supplemented with 10% FBS and differentiated by a reduced-serum media supplemented with 1% FBS and 20µM of retinoic acid (RA) for 7-10 days. Cells were cultured under 5% CO2 at 37ºC and subjected to reduced serum and RA for 7-10 days to differentiate into neurons prior to any experimentation[GU1] . For 5kPa and 1kPa O2 levels, cells were cultured in a chamber set to physioxic or hypoxic O2 for four and one day(s), respectively, prior to data collection.

Electrophysiology: Whole-cell currents and action potentials were recorded using a MultiClamp 700B/HEKA EPC10 amplifier for data acquisition (n=10 cells per condition) and analysis was performed with Clampex 11.2 (Molecular Devices)/Patchmaster (HEKA) software. Whole-cell currents were recorded in HEPES buffered standard solution at a perfusion rate of 4ml/min and ~35ºC in the respective 1kPa, 5kPa or 21kPa O2 environments.

Statistical Analysis: Whole-cell current amplitudes were analysed with a two-way ANOVA and half-activation voltages, and action potential amplitudes were compared using Student's t-tests ($p<0.05$ was considered significant). Data is presented as mean ± SEM.

Results and Conclusions:

Physioxia significantly increased TEA-sensitive K^+ currents (amplitudes at +50mV: 21kPa: 205.9±39.6pA; 5kPa: 240.6±67.3pA, $p<0.001$) and shifted half-activation voltages to hyperpolarised values (V1/2 K^+: 21kPa: 13.8±2.0mV; 5kPa: 3.6±3.1mV, $p=0.01$). Voltage-gated Na^+ currents were enhanced under physioxia (amplitude at 0mV: 21kPa: -93.2±23.9pA; 5kPa: -143.6±23.0pA, $p=0.001$) without displaying a changed voltage activation curve (V1/2 Na^+: 21kPa: -14.3±1.9mV; 5kPa: -12.6±2.3mV, $p=0.59$). Preliminary data indicate that K^+ currents are strongly diminished under hypoxic conditions. Action potential amplitudes were affected by ambient O2 levels resulting in lower values at 5kPa following 300pA current injection at a holding potential of -60mV (21kPa: 22±2mV; 5kPa: 17±0.4mV, $p<0.05$) in physioxia, indicating that cells in physiological oxygen levels possess different ion channel regulation and electrophysiological phenotypes than under hyperoxic conditions.

These findings demonstrate that physiological oxygen levels critically shape neuronal ion channel function and excitability, underscoring the need to consider physioxia in neurophysiological studies and vascular dementia research. Understanding oxygen-dependent ion channel regulation may inform therapeutic strategies for vascular dementia and other hypoxia-related neurological disorders

[GU1]I am not sure I understand why this is important?

C20

Choroid plexus volume increases in Alzheimer's disease genetic risk: an early marker of glymphatic dysfunction?

Hannah Chandler[1], Natalie Jones[1], Neil Harrison[1], Kevin Murphy[1], Thomas Lancaster[2]

[1]CUBRIC, Cardiff University , Wales, UK, [2]University of Bath, England, UK

Introduction

The choroid plexus (CP) is a highly vascularised structure comprised of a complex network of capillaries that produce cerebrospinal fluid (CSF) via ependymal cells lining the brains ventricles[1]. The CP serves as a critical interface between the brain and periphery, regulating CSF production, maintaining the blood-CSF barrier, and mediating neuroimmune signalling. Structural and functional alterations of the CP are implicated in early neurodegeneration, particularly in AD, where disrupted CSF dynamics, impaired amyloid clearance, and neuroinflammation contribute to disease progression. Polygenic risk scores for AD (AD-PRS) help quantify cumulative genetic risk across thousands of common variants as a preclinical maker of future AD susceptibility, however, the relationship between AD-PRS and CP structure remains unexplored. Recent work also highlights the importance of cellular context in genetic risk. I.e. different brain cell types contribute distinctively to AD-related pathways, including vascular, glial, and barrier-related processes.[2]

Aims/Objectives

Here, we adopt a cell-specific PRS framework, integrating genome-wide summary statistics with transcriptional profiles, enabling investigation of genetic risk partitioned by a range of neural cell species. We examined associations between whole-genome AD-PRS, cell-type-specific AD-PRS, and CP volume. We hypothesise that CP volume would be associated with AD-PRS, particularly the ependymal cell-specific PRS. We suggest this will reflect the specific AD-linked gene expression profile of ependymal cells that uniquely feature in the CP epithelial lining.[2]

Methods

In a UK Biobank (UKBB) sample (*n*=31,943) we used the CP volume image derived phenotype, derived using T1-weighted MRI and the FreeSurfer pipeline[3], which segments the CP within the lateral ventricles. We calculated two PRS:

1. Whole-genome AD-PRS, excluding *APOE* and major histone compatibility (*MHC*) regions to focus on genome-wide contributions

beyond the major risk loci and complex linkage disequilibrium structure, respectively.

2. Cell-type-specific AD-PRS, computed for 16 brain and vascular-associated cell types (including ependymal, astrocyte, oligodendrocyte, endothelial, pericyte, and smooth muscle cell classes).[1]

All AD-PRS were generated using gtx, integrating AD summary statistics with cell-type-enriched transcriptomic profiles drawn from [1] who characterized transcriptional signatures across vascular, immune, and neural cell populations in postmortem human brain tissue. The analytic framework follows our recent study that tests associations between imaging phenotypes and polygenic scores derived both genome-wide and at the cell-type level.[4]

Results

The whole-genome AD-PRS (excluding *APOE/MHC* regions) was positively associated with CP volume (β=0.0076,SE=0.004,*p*=0.041, Figure1,left), indicating that global AD-PRS contributes to variation in CP structure. Among cell-specific PRS, ependymal cell AD-PRS showed a robust, highly specific positive association with CP volume (β=0.0499,SE=0.0231,*p*=0.016, Figure1,center). This association was empirically larger than all other cell-type-specific PRS (Z=1.62,*p*=0.034, Figure1,right).

Conclusion

Both whole-genome and ependymal cell-specific polygenic risk for AD are associated with CP volume, with the strongest and most specific effect observed for the ependymal PRS. Ependymal cell-specific polygenic risk is selectively and positively associated with CP volume. This highlights a mechanistic link between genetic vulnerability and CP volume, demonstrating cell-type-informed genetic analysis can reveal tissue-specific alterations of AD-related polygenic risk. CP volume represents a promising imaging biomarker for investigating the biological pathways through which genetic risk for AD manifests in the aging brain.

Ethics: Full ethical approval for all data collection by UKBB team.

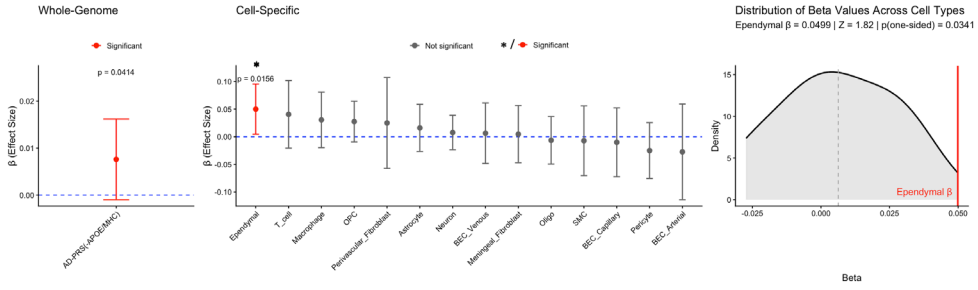

C21

Defective autophagy impairs endothelial cell function and blood-brain barrier integrity.

Eleonora Mameli[1], Phoebe Philpott[1], Nick Verity[1], Audrey Chagnot[1], Axel Montagne[1], Spartaco Santi[2], Maurits Jansen[3], Eva Jover[4], Giles Hardingham[1], Andrea Caporali[1]

[1]University of Edinburgh, United Kingdom, [2]CNR Institute of Molecular Genetics Bologna, ITALY, [3]University of Virginia , USA, [4]Navarrabiomed Pamplona, Spain

Cerebral small vessel disease (cSVD) is a common type of vascular dementia marked by dysfunction in brain endothelial cells (BECs), which leads to changes in white matter, an early sign of the disease. Endothelial dysfunction occurs before the blood-brain barrier (BBB) breaks down [1]. Identifying new genes linked to this dysfunction can improve our understanding of BECs in BBB integrity. A key factor in BBB disruption is the overproduction of matrix metalloproteinases due to neurovascular inflammation. While autophagy is associated with neurodegenerative diseases and inflammation, its role in endothelial barrier function in cSVD is still unclear. Increasing evidence suggests that proper autophagic flux in ECs is crucial for maintaining vascular function, while defective autophagy can lead to a pro-inflammatory phenotype in these cells [2]. We previously demonstrated that the centriolar protein trichoplein (TCHP) plays a critical role in connecting EC function with autophagy regulation. The loss of TCHP is associated with impaired autophagy and increased inflammation in ECs [3].

Here, we propose to investigate the role of TCHP in the mechanisms underlying defective autophagy, EC inflammation, and increased BBB permeability.

We then generated endothelial-specific Tchp knock-out mice ($Tchp^{EC}$). Using a labelled dextran injection and magnetic resonance imaging to map and quantify BBB permeability in $Tchp^{EC}$ mice revealed a significant increase in hippocampal vascular permeability compared to wild type (WT) mice (Gd DTPA mM: 0.83±0.16 WT vs 1.13±0.25 $Tchp^{EC}$; n=8 unpaired t-test 0.037). $Tchp^{EC}$ mice showed a decrease in pericytes coverage (CD13%: 21.26±6.10 WT vs 13.96±5.09 $Tchp^{EC}$; n=7 unpaired t-test 0.032) and capillary diameters (µm: 2.99±0.21 WT vs 3.34±0.31 $Tchp^{EC}$; n=7 unpaired t-test 0.029). Transcriptomics analysis of BEC sorted from WT and $Tchp^{EC}$ mice showed that the Gene Ontology terms cytokine-mediated signalling pathway, extracellular matrix organisation, and chemokine-mediated signalling pathway are enriched in BECs from $Tchp^{EC}$ mice. Gelatin zymography further confirmed increased Mmp9 production in $Tchp^{EC}$ BECs (1.02±0.21 WT vs 1.44±0.26 $Tchp^{EC}$; n=7 unpaired t-test 0.007). Furthermore, we used a co-culture cellular model using WT pericytes and $Tchp^{EC}$ BECs to identify key pathways affected in pericytes by the loss of Tchp in BECs. Transcriptomics analysis revealed that the Notch pathway is significantly affected in pericytes when co-cultured with $Tchp^{EC}$ BECs. Finally, treatment of $Tchp^{EC}$ mice with a MMP9 inhibitor (GM6001, i.p. 50mg/Kg every second day for 15 days) restored pericyte coverage (CD13%: 19.46±1.53 WT; 12.38±2.77 $Tchp^{EC}$; 16.28±2.67 $Tchp^{EC}$+*GM*; n=7 two-way Anova $p<0.01$) and reduced BBB permeability(Permeability index; relative fluorescent unit/gr tissue 106.73±46.63 WT; 270.23±22.80 $Tchp^{EC}$; 173.14±33.18 $Tchp^{EC}$+*GM*; n=7 two-way Anova $p<0.01$).

In conclusion, our data indicate that TCHP-induced defective autophagy in endothelial cells may result in inflammation and compromised blood-brain barrier integrity.

All experiments involving mice were performed following the guidance and operation of the Animals (Scientific Procedures) Act 1986 and the prior approval of the UK Home Office and the University of Edinburgh Animal Welfare and Ethical Review Board.

C24

A flow-diffusion model of capillary oxygen transport for the robust and minimally invasive estimation of venous cerebral blood volume from MR relaxometry

Stefano Zappala[1], Eleonora Patitucci[2], Fabian Küppers[3], Jon Shah[4], Richard Wise[5], Michael Germuska[6]

[1]Cardiff University Brain Research Imaging Centre (CUBRIC), School of Computer Science and Informatics, Cardiff University, Cardiff, United Kingdom, United Kingdom, [2]Cardiff University Brain Research Imaging Centre (CUBRIC), School of Psychology, Cardiff University, Cardiff, United Kingdom, United Kingdom, [3]Institute of Neuroscience and Medicine 4, Forschungszentrum Juelich, Juelich, Germany, Germany, [4]Department of Neurology, Department of Neurology, RWTH Aachen University, Aachen, Germany, Germany, [5]Department of Neurosciences, Imaging and Clinical Sciences, University 'G.d'Annunzio' of Chieti-Pescara, Chieti, Italy, Italy, [6]Department of Radiology, University of California Davis Medical Center, Sacramento, CA, United States of America, United States of America, United States of America

Introduction

Oxygen Extraction Fraction (OEF) and venous Cerebral Blood Volume (vCBV) provide crucial insight into brain oxygen metabolism, but their co-linearity in the qBOLD model leads to unstable estimations. We address this by integrating a flow-diffusion model of oxygen transport into the qBOLD framework (1), which introduces physiological priors derived from quantitative perfusion maps (2) (via ASL (5)). This approach stabilizes the OEF and vCBV estimations while requiring only ASL as additional input (3,4). Building on the recent successful application of a highly sensitive GE-SE EPIK sequence (Kuppers et al. (6)) for rapid vCBV estimation, we integrated our flow-diffusion model to stabilize the direct vCBV estimations derived from the qBOLD equations applied to the GE-SE EPIK signal.

Methods

All data were acquired using two 3T Siemens Prisma scanners with 32-channel head coils. 21 healthy participants (mean age 31.9+-6.5 years) took part in the study. Scanning session included structural MPRAGE (1mm iso), the rapid GE-SE EPIK sequence (10 echoes, 1.9x1.9x3.3mm^3, acquisition time <2 min (6)), and perfusion imaging via Velocity-Selective Arterial Spin Labeling (VS-ASL, 3.3x3.3x6.0mm^3, acquisition time <5 min (5)). The GE-SE EPIK and VS-ASL measurements were conducted during two separate 10-minute isometabolic hypercapnic gas challenges (5% CO2). This allowed the quantitative measurement of vCBV increase consistent with the Grubb relationship (9) $(CBF/CBF0)^{alpha}$, where CBF0 is perfusion in baseline, with an exponential alpha of 0.38 in animal model or 0.18 in healthy subjects (10). Non-linear least-squares fitting of the qBOLD model (Equations 1 and 2 in Figure 3) gave vCBV and OEF maps (Equation 3).

Results & Discussion

Figure 2 displays the vCBV maps for a representative healthy participant at baseline (left) and during hypercapnia (right). The vCBV values exhibit good contrast across the grey matter (GM) area. However, vCBV estimations in white matter (WM) show a slight bias against the expected reduced values relative to

GM, likely due to non-blood sources of susceptibility. Inhomogeneities are also noticeable within the WM when transitioning between anterior and posterior regions. The average vCBV (in [%]) for the healthy cohort is summarized in Figure 3: reported ROIs are left and right frontal (Front), parietal (Par), temporal (Temp) and occipital (Occ). Baseline vCBV was measured at 2.64+-0.22% (mean +- standard deviation over normal-appearing GM), consistent with literature. A significant increase in vCBV to 2.82+-0.29% was observed during the hypercapnic modulation (left side of Figure 3) as a result of the induced hyperemia (CBF increased by 34.68+-13.92% from a baseline of 55.50+-12.54 ml/100g/min). This vCBV increase aligns closely with the Grubb relationship, as shown on the right side of Figure 3: our study result (1.0716+-0.999) is near the expected increase with alpha=0.18 (1.0543+-0.0190 (10)).

Conclusion

The flow-diffusion model successfully regularised the estimation of vCBV directly from fast GE-SE MR signal measurements, requiring only additional ASL-based perfusion maps. GM values for vCBV were consistent with established literature, demonstrating sensitivity to both altered physiological conditions and pathology. With further refinement, this method offers the potential for rapid, accurate, and non-invasive measurement of tissue oxygenation, enabling clear clinical translation.

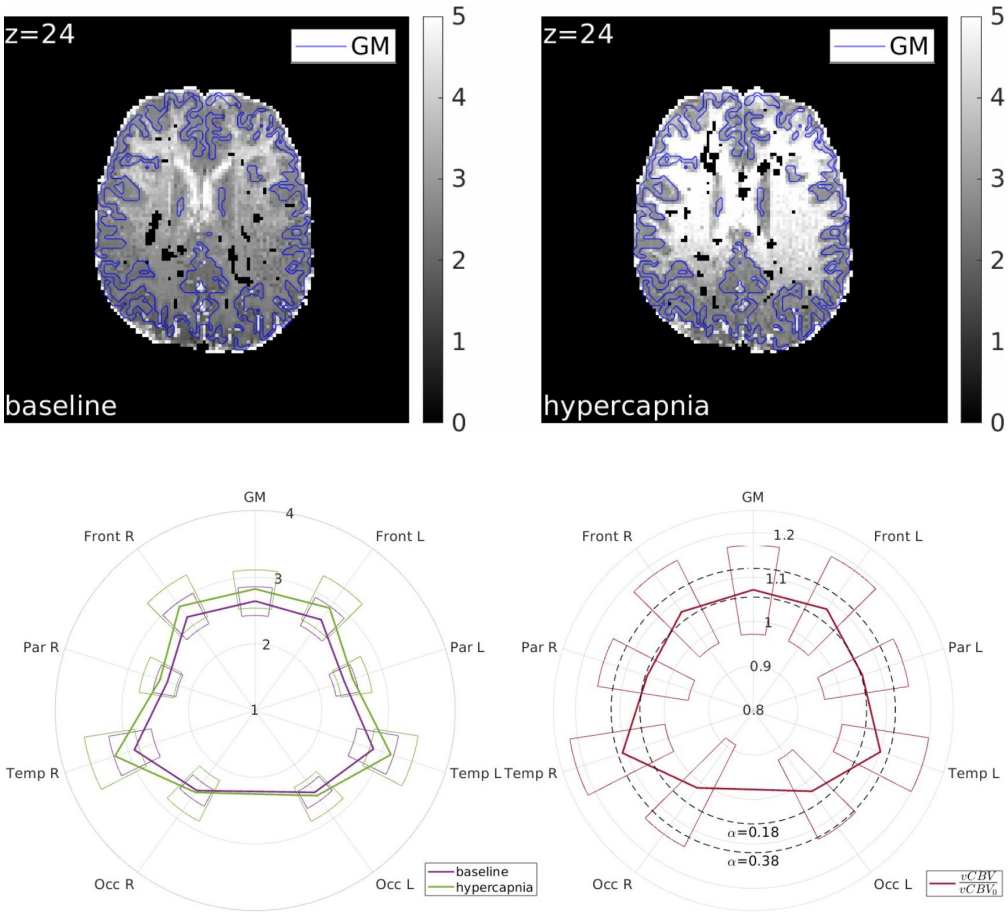

$$S(t) = \begin{cases} S_0 \cdot e^{vCBV} \cdot e^{-t \cdot R_2^*} & for\ 0 < t < \frac{1}{2}TE_{SE1} \\ \frac{S_0}{\delta} \cdot e^{vCBV} \cdot e^{-TE_{SE1}(R_2^* - R_2)} \cdot e^{-t(2 \cdot R_2 - R_2^*)} & for\ \frac{1}{2}TE_{SE1} < t \leq TE_{SE1} \\ \frac{S_0}{\delta} \cdot e^{vCBV} \cdot e^{+TE_{SE1}(R_2^* - R_2)} \cdot e^{-tR_2^*} & for\ TE_{SE1} < t < \frac{1}{2}(TE_{SE1} + TE_{SE2}) \\ S_0 \cdot e^{vCBV} \cdot e^{-TE_{SE2}(R_2^* - R_2)} \cdot e^{-t(2 \cdot R_2 - R_2^*)} & for\ \frac{1}{2}(TE_{SE1} + TE_{SE2}) < t \leq TE_{SE2} \end{cases} \quad (1)$$

$$OEF = \frac{{R_2}^* - R_2}{\frac{4}{3}\pi \cdot \gamma \cdot vCBV \cdot \Delta\chi_0 \cdot Hct \cdot B_0} \quad (2)$$

$$vCBV = \rho \cdot \frac{C_aO_2 \cdot CBF \cdot OEF}{k \cdot \left(P_{50} \cdot \sqrt[h]{\frac{2}{OEF} - 1} - P_mO_2\right)} \quad (3)$$

S_0	MR Signal at time zero	estimated
δ	Refocusing Pulse Imperfection Factor	estimated
TE_{SE1}, TE_{SE2}	Echo times for the two SEs	TE_{SE1}=57ms, TE_{SE2}=114ms
${R_2}^*$, R_2	Effective and Transverse Relaxation Rate	estimated
γ	Gyromagnetic ratio of the proton	268 106 rad/s/T
$\Delta\chi_0$	Magnetic susceptibility difference between fully oxygenated and fully deoxygenated blood	0.264 ppm
Hct	Fractional haematocrit	extracted with assumed haemoglobin = 14g/dL
ρ	Ratio between blood volume containing deoxyhaemoglobin and capillary blood volume	2.5
k	Effective O_2 permeability	$3\,\mu mol/mmHg/ml/min$
h	Hill constant	2.84
P_{50}	Oxygen partial pressure when half of hemoglobin is saturated with oxygen	$26 mmHg$
P_mO_2	Mitochondrial partial O_2 pressure	$0\,mmHg$
C_aO_2	Concentration of oxygen in arteries	extracted with assumed haemoglobin = 14g/dL

C25

The M5 muscarinic receptor: a potential target in cerebrovascular disorders and vascular dementia?

Aisling McFall[1], Nicola Gilroy[1], Lorraine Work[1]

[1]University of Glasgow, Scotland, UK

The vascular contributions to cognitive impairment and dementia (VCID) have been recognised as a research priority [1]. Current treatments for cognitive deficits in Alzheimer's Disease centre on rescuing cholinergic transmission with acetylcholinesterase inhibitors, for example donepezil. Importantly, there is evidence that donepezil can also have a benefit on cognition in vascular dementia (VaD) and patients with vascular cognitive impairment [2-4], indicating that the cholinergic system can directly impact on cognition in cerebrovascular disorders. Of the five muscarinic acetylcholine (ACh) receptor subtypes (M1-M5), the M5 receptor has been suggested to play a role in cerebral blood flow (CBF) regulation [5,6]. Here, it was hypothesised that M5 receptor expression would be enriched in the cerebrovasculature of rat brains.

Whole brain (WB) homogenates from stroke prone spontaneously hypertensive rats (SHRSP), underwent a vessel enrichment protocol using a ficoll gradient. Cerebral and peripheral vessels were also dissected from SHRSP, namely the middle cerebral artery, basilar, transcending aorta, carotid and mesenteric arteries. RNA was isolated from WB homogenates, vessel enriched fractions (S1) and individual vessels. qPCR used to determine the expression levels of M5 & M3 muscarinic receptors along with claudin-5 tight junction protein and aquaporin 4 (AQP4) (expressed predominantly on astrocyte end-feet) relative to the housekeeping gene b-actin. Data was analysed using a paired t-test and $p<0.05$ was considered statistically significant.

M5 expression was significantly 66% higher in S1 fractions compared to WB ($p=0.01$) while M3 expression appeared to increase by 95% although this was not statistically significant ($p=0.08$) (Figure 1). Claudin-5 and AQP4 were significantly increased in S1 fractions by 1800% ($p=0.0007$) and 65% ($p=0.03$) respectively, confirming vasculature enrichment in the samples. Further to this, M5 expression was significantly between 82 and 166-fold ($p<0.01$), 22 and 45-fold ($p<0.05$), and 74 and 150-fold ($p<0.01$ and $p<0.0001$) greater in the MCA and basilar artery of the SHRSP rat compared to the aorta, carotid and mesenteric arteries, respectively (Figure 2). M3 expression, however, was similar across all arteries assessed with the exception of a 3-fold increase in expression in the mesenteric vs the basilar artery ($p<0.05$).

In SHRSP brains, the M5 muscarinic receptor expression is significantly enriched in the cerebrovasculature in both vessel enriched brain fractions and when assessing expression in dissected vessels. This may suggest an important role of M5 in the cerebrovasculature which may provide a potential novel therapeutic target for improving CBF in cerebrovascular disorders and VaD.

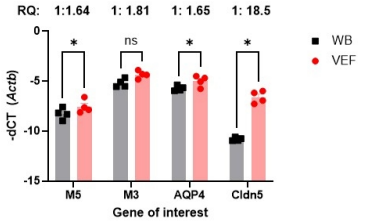

Figure 1. qPCR expression data demonstrating statistically significant increased expression of M5 muscarinic receptor and genes of the neurovascular unit (aquaporin 4 (AQP4, astrocytes) and claudin-5 (Cldn5, endothelial cells)), but not the M3 muscarinic receptor, in vessel enriched fractions (VEF) compared to whole brain homogenate (WB) from the brains of stroke prone spontaneously hypertensive rats (n=4). Relative quantification values indicating expression compared to WB are shown (RQ). VEF fractions were prepared using a ficoll gradient. Data analysed with individual paired t-tests.*p<0.05, ***p<0.001.

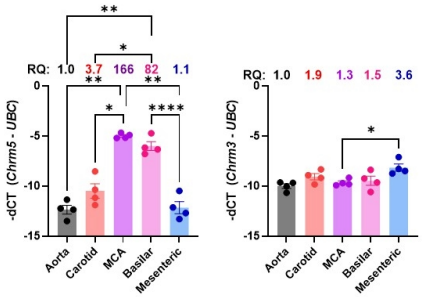

Figure 2. qPCR expression data of M5 muscarinic receptor (A) and M3 muscarinic receptor (B) in vessels isolated from SHRSP demonstrating increased expression of M5 in cerebral vessels compared to peripheral vessels while M3 expression did not differ between cerebral and peripheral vessels bar a slight increase in the mesenteric artery (n=4)